comptes rendus palevol

2023 • 22 • 32

Limb histology of the Triassic stem turtles *Proterochersis porebensis* Szczygielski & Sulej, 2016 and *Proganochelys quenstedtii* Baur, 1887 with insights into growth patterns of early turtles

Tomasz SZCZYGIELSKI, Nicole KLEIN,
Justyna SŁOWIAK-MORKOVINA & Torsten M. SCHEYER

art. 22 (32) — Published on 6 November 2023
www.cr-palevol.fr

PUBLICATIONS SCIENTIFIQUES

MUSÉUM NAL HIST NATURELLE

Comptes Rendus Palevol est indexé dans / Comptes Rendus Palevol *is indexed by:*
– Cambridge Scientific Abstracts
– Current Contents® Physical
– Chemical, and Earth Sciences®
– ISI Alerting Services®
– Geoabstracts, Geobase, Georef, Inspec, Pascal
– Science Citation Index®, Science Citation Index Expanded®
– Scopus®.

Les articles ainsi que les nouveautés nomenclaturales publiés dans *Comptes Rendus Palevol* sont référencés par / *Articles and nomenclatural novelties published in* Comptes Rendus Palevol *are registered on:*
– ZooBank® (http://zoobank.org)

Comptes Rendus Palevol est une revue en flux continu publiée par les Publications scientifiques du Muséum, Paris et l'Académie des sciences, Paris
Comptes Rendus Palevol *is a fast track journal published by the Museum Science Press, Paris and the Académie des sciences, Paris*

Les Publications scientifiques du Muséum publient aussi / *The Museum Science Press also publish:*
Adansonia, ***Geodiversitas***, ***Zoosystema***, ***Anthropozoologica***, ***European Journal of Taxonomy***, ***Naturae***, ***Cryptogamie*** **sous-sections** ***Algologie***, ***Bryologie***, ***Mycologie***.

L'Académie des sciences publie aussi / *The Académie des sciences also publishes:*
Comptes Rendus Mathématique, Comptes Rendus Physique, Comptes Rendus Mécanique, Comptes Rendus Chimie, Comptes Rendus Géoscience, Comptes Rendus Biologies.

Diffusion – Publications scientifiques Muséum national d'Histoire naturelle
CP 41 – 57 rue Cuvier F-75231 Paris cedex 05 (France)
Tél. : 33 (0)1 40 79 48 05 / Fax : 33 (0)1 40 79 38 40
diff.pub@mnhn.fr / https://sciencepress.mnhn.fr

Académie des sciences, Institut de France, 23 quai de Conti, 75006 Paris.

ISSN (imprimé / *print*) : 1631-0683/ ISSN (électronique / *electronic*) : 1777-571X

Limb histology of the Triassic stem turtles *Proterochersis porebensis* Szczygielski & Sulej, 2016 and *Proganochelys quenstedtii* Baur, 1887 with insights into growth patterns of early turtles

Tomasz SZCZYGIELSKI
Institute of Paleobiology, Polish Academy of Sciences,
Twarda 51/55, 00-818 Warsaw (Poland)
t.szczygielski@twarda.pan.pl (corresponding author)

Nicole KLEIN
Palaeontological Institute and Museum, University of Zurich,
Karl-Schmid-Strasse 4, 8006 Zurich (Switzerland)
and Institute of Geosciences, Paleontology, University of Bonn,
Nussallee 8, 53115 Bonn (Germany)
nklein@posteo.de

Justyna SŁOWIAK-MORKOVINA
Institute of Paleobiology, Polish Academy of Sciences,
Twarda 51/55, 00-818 Warsaw (Poland)
justyna.slowiak@twarda.pan.pl

Torsten M. SCHEYER
Department of Palaeontology, University of Zurich,
Karl-Schmid-Strasse 4, 8006 Zurich (Switzerland)
tscheyer@pim.uzh.ch

Submitted on 22 February 2023 | Accepted on 9 June 2023 | Published on 6 November 2023

urn:lsid:zoobank.org:pub:D239F3CA-095A-4EE5-8F12-F96402E628CC

Szczygielski T., Klein N., Słowiak-Morkovina J. & Scheyer T. M. 2023. — Limb histology of the Triassic stem turtles *Proterochersis porebensis* Szczygielski & Sulej, 2016 and *Proganochelys quenstedtii* Baur, 1887 with insights into growth patterns of early turtles. *Comptes Rendus Palevol* 22 (32): 635-665. https://doi.org/10.5852/cr-palevol2023v22a32

ABSTRACT
Data on turtle limb bone histology and microstructure are spotty, especially for Mesozoic taxa, despite significant progress made in recent years. Here we provide first detailed information on the stylopodia of the Late Triassic stem turtles *Proganochelys quenstedtii* Baur, 1887 from Switzerland and *Proterochersis porebensis* Szczygielski & Sulej, 2016 from Poland. In both taxa we observed large, internal medullary regions filled with endosteal trabeculae and poorly to moderately vascularized parallel-fibered (grading locally to lamellar) periosteal cortices. Primary vasculature is predominantly longitudinal, in *Proterochersis porebensis* locally with radial inclination. In large specimens, secondary remodeling is significant in the deeper cortex, but it neither completely obliterates the primary tissue nor reaches the external surface of the bone in either taxon. Comparison of histological data, limb morphology, shell and limb lengths as well as proportions reveal differences in growth patterns between the taxa: *Proganochelys quenstedtii* seems to grow faster during early life stages than *Proterochersis porebensis* and attained distinctly larger body sizes earlier in ontogeny, even though the asymptotic body size is roughly the same for both species. Overall, the histological and microstructural characteristics of stylopodial bones of Triassic turtles more closely resemble those of more recent representatives of that group than earlier stem turtles.

KEY WORDS
Humerus, femur, histology, microstructure, *Proterochersis*, *Proganochelys*, turtle, Testudinata, Triassic, Norian.

RÉSUMÉ
Histologie des membres des tortues souches du Trias Proterochersis porebensis Szczygielski & Sulej, 2016 *et* Proganochelys quenstedtii Baur, 1887 *avec un aperçu des schémas de croissance des premières tortues.* Les données sur l'histologie et la microstructure des os des membres des tortues sont inégales, en particulier pour les taxons du Mésozoïque, malgré les progrès significatifs réalisés ces dernières années. Nous fournissons ici les premières informations détaillées sur les stylopodes des tortues souches du Trias supérieur *Proganochelys quenstedtii* Baur, 1887 de Suisse et *Proterochersis porebensis* Szczygielski & Sulej, 2016 de Pologne. Chez les deux taxons, nous avons observé de grandes régions médullaires internes remplies de trabécules endo-osseuses et des cortex périostés à fibres parallèles faiblement à modérément vascularisés (évoluant localement à lamellaires). La vascularisation primaire est principalement longitudinale, chez *Proterochersis porebensis* elle est localement radiale. Dans les grands spécimens, le remodelage secondaire est significatif dans le cortex plus profond, mais il n'efface pas complètement le tissu primaire, ni n'atteint la surface externe de l'os dans l'un ou l'autre des taxons. La comparaison des données histologiques, de la morphologie des membres, de la longueur de la coquille et des membres, ainsi que des proportions, révèle des différences dans les schémas de croissance entre les taxons : *Proganochelys quenstedtii* semble croître plus rapidement au cours des premiers stades de la vie, par rapport à *Proterochersis porebensis*, et atteint des tailles corporelles nettement plus grandes plus tôt dans l'ontogénie, même si la taille asymptotique du corps est à peu près identique pour les deux espèces. Dans l'ensemble, les caractéristiques histologiques et microstructurales des os stylopodiaux des tortues du Trias ressemblent davantage à celles des représentants plus récents de ce groupe que les tortues plus anciennes du groupe souche.

MOTS CLÉS
Humérus, fémur, histologie, microstructure, *Proterochersis*, *Proganochelys*, tortue, Testudinata, Trias, Norien.

INTRODUCTION

Research of turtle limb bone histology has a long history with the earliest accounts (Quekett 1849a, b, 1855) mostly noting the large size of the osteocytes, the compactness of the cortices, and the cancellous interior of extant turtle limb bones. Probably the first more in-depth descriptions of turtle femur histology are those of Foote (1911, 1916), who also pointed out reduced medullary cavities frequently filled with cancellous bone and thick, compact cortices with a lamellar-zonal arrangement of tissue. Wallis (1927) provided additional data on limb bone histology, noting that the cortices are composed predominantly of parallel-fibered bone, and also described bone healing in turtles. Gross (1934), in his work on fossil reptile and amphibian bone histology, noted the scarcity of fossilized turtle limb material and described extant turtle limbs instead, mostly repeating the observations of previous authors. Mattox (1936) was probably the first to notice the presence of annular growth marks in the turtle long bones and their potential utility for skeletochronological estimation of an approximate age of the individual – a conclusion followed by subsequent research (Peabody 1961; Hammer 1969; Castanet & Cheylan 1979; Cheylan 1981; MacCulloch & Secoy 1983; Castanet 1985, 1987, 1988, 1994; Zug & Balazs 1985; Zug *et al.* 1986, 1995, 1997, 2002, 2006; Zug 1990; Klinger & Musick 1992, 1995; Chaloupka & Musick 1997; Parham & Zug 1997; Zug & Glor 1998; Bjorndal *et al.* 1998; Coles *et al.* 2001; Snover 2002; Snover & Hohn 2004; Ehret 2007; Avens & Goshe 2007; Snover *et al.* 2007a, b; Chinsamy & Valenzuela 2008; Snover & Rhodin 2008; Curtin *et al.* 2008; Goshe *et al.* 2009, 2010; Casale *et al.* 2011; Avens *et al.* 2012, 2013, 2015; Petitet *et al.* 2012; Avens & Snover 2013; Turner Tomaszewicz *et al.* 2015; Çiçek *et al.* 2016; Lenz *et al.* 2016; Schucht *et al.* 2021). Balli (1937), Haines (1938, 1969), Crawford (1940), Enlow & Brown (1957), Suzuki (1963), and Ricqlès (1976) provided further reports of turtle limb bone histology, microstructure, and development during ontogenesis. Enlow (1969) improved on that, presenting a more thorough description, and noted that the cancellous bone in turtles tends to show little to no remodeling with much of the primary tissue being preserved in between the intertrabecular spaces. Rhodin *et al.* (1980, 1981) characterized some aspects of limb histology and microstructure of *Dermochelys coriacea* (Vandelli, 1761). That was expanded upon by Rhodin (1985) in a broader context of aquatic turtle evolution and growth rate including, probably for the first time, remarks on limb histology of fossil turtles, in particular *Archelon ischyros* Wieland, 1896, *Rhinochelys pulchriceps* (Owen, 1842) (Owen 1851), and *Stupendemys geographicus* Wood, 1976 (Enlow & Brown 1957 earlier presented thin sections of femora of some Eocene species, but these were not identified taxonomically), and a follow-up study on that subject was performed by Rhodin (1996). Montes *et al.* (2007, 2010) and Cubo *et al.* (2008, 2012) provided data on bone growth rates in turtles. A number of authors tackled the question of the unclear correlation between the limb microstructure and habitat in turtles (Ricqlès *et al.* 2004; Germain & Laurin 2005; Kriloff *et al.* 2008; Canoville & Laurin 2010; Laurin *et al.* 2011; Houssaye 2013; Nakajima *et al.* 2014; Pereyra 2022). Gônet *et al.* (2023) studied the correlation between the femoral microstructure and locomotion in bipedal, facultatively bipedal, and quadrupedal reptiles, including turtles. Thorough studies of histology across different limb bones and ontogenetic stages were performed for extant species by Botha

TABLE 1. — Visual documentation (thin section photographs, CT data, binary images of density, drawings) of testudinate long bone histology and microstructure available in published literature.

Taxon	References
Stem	
Proganochelys quenstedtii	Nakajima 2017; Schoch *et al.* 2019
Sichuanchelyidae	Nakajima 2017
Xinjiangchelyidae	Danilov *et al.* 2018
Cryptodira	
Carettochelyidae	Rhodin 1985; Nakajima *et al.* 2014
Chelonioidea	Quekett 1849b; Balli 1937; Amprino & Godina 1947; Rhodin *et al.* 1980, 1981, 1996; Rhodin 1985; Zug *et al.* 1986, 2006; Klinger & Musick 1992; Zug & Parham 1996; Bjorndal *et al.* 1998; Coles *et al.* 2001; Snover 2002; Wilson 2023; Snover & Hohn 2004; Ricqlès *et al.* 2004; Avens & Goshe 2007; Snover *et al.* 2007a, b; Snover & Rhodin 2008; Kriloff *et al.* 2008; Avens *et al.* 2009, 2012, 2013, 2015; Goshe *et al.* 2009, 2010; Casale *et al.* 2011; Laurin *et al.* 2011; Petitet *et al.* 2012; Houssaye 2013; Avens & Snover 2013; Nakajima *et al.* 2014; Turner Tomaszewicz *et al.* 2015; Lenz *et al.* 2016
Chelydridae	Foote 1911, 1916; Enlow & Brown 1957; Peabody 1961; Enlow 1969; Hammer 1969; Horner *et al.* 2001; Canoville & Laurin 2010; Laurin *et al.* 2011; Nakajima *et al.* 2014; Gônet *et al.* 2023; Valastro *et al.* 2023
Emydidae	Foote 1916; Wallis 1927; Haines 1942, 1969; Enlow & Brown 1957; Suzuki 1963; Enlow 1969; Castanet 1985; Rhodin 1985; Snover & Rhodin 2008; Laurin *et al.* 2011; Nakajima *et al.* 2014; Çiçek *et al.* 2016
Geoemydidae	Nakajima *et al.* 2014; Schucht *et al.* 2021
Kinosternidae	Foote 1916; Enlow & Brown 1957; Laurin *et al.* 2011; Nakajima *et al.* 2014
Protostegidae	Wilson 2023
Testudinidae	Foote 1916; Haines 1938; Crawford 1940; Amprino & Godina 1947; Enlow & Brown 1957; Enlow 1969; Ricqlès 1976; Castanet & Cheylan 1979; Cheylan 1981; Castanet 1988, 1994; Ricqlès *et al.* 2004; Ehret 2007; Kriloff *et al.* 2008; Canoville & Laurin 2010; Laurin *et al.* 2011; Nakajima *et al.* 2014; Botha 2017; Botha & Botha 2019; Bhat *et al.* 2019, 2023; Pereyra *et al.* 2019; Pereyra 2022; Gônet *et al.* 2023
Toxochelyidae	Wilson 2023
Trionychidae	Foote 1916; Cubo *et al.* 2008; Montes *et al.* 2010; Laurin *et al.* 2011; Nakajima *et al.* 2014
Indeterminate fossil	Bailleul *et al.* 2011
Pleurodira	
Araripemydidae	Sena *et al.* 2021
Chelidae	Laurin *et al.* 2011; Nakajima *et al.* 2014; Pereyra *et al.* 2019, 2020; Pereyra 2022
Pelomedusidae	Haines 1969; Kriloff *et al.* 2008; Laurin *et al.* 2011
Podocnemididae	Enlow 1969; Chinsamy & Valenzuela 2008; Nakajima *et al.* 2014; Cadena *et al.* 2020
Unspecified extant and fossil	Cerda *et al.* 2020
Indeterminate fossil	Enlow & Brown 1957; Danilov *et al.* 2018

(2017) and Botha & Botha (2019) for *Stigmochelys pardalis* (Bell, 1828), by Bhat *et al.* (2019) for *Chersina angulata* (Schweigger, 1812), by Pereyra *et al.* (2020) for *Hydromedusa tectifera* Cope, 1869, and by Pereyra (2022) for *Hydromedusa tectifera*, *Phrynops hilarii* (Duméril & Bibron, 1835), and *Chelonoidis chilensis* (Gray 1870). Pereyra *et al.* (2019) described histological correlates of muscle attachments on the pectoral girdle and humerus in extant terrestrial and aquatic turtles and Valastro *et al.* (2023) documented the healing process of a complex humeral fracture in a juvenile *Caretta caretta* (Linnaeus, 1758). Bhat *et al.* (2023) focused on the differences in tibial histology in *Chersina angulata* from different localities covering the timespan from the late Miocene to Recent, particularly in the context of growth tempo.

Intriguingly, representatives of completely extinct genera were largely ignored as a source for appendicular osteohistological data, and only very recently gained some attention thanks to the works on *Annemys* sp. and another Middle Jurassic turtle from Russia by Danilov *et al.* (2018), *Araripemys barretoi* Price, 1973 by Sena *et al.* (2021), *Desmatochelys lowii* Williston, 1894 and *Protostega gigas* Cope, 1871 by Wilson (2023), *Stupendemys geographicus* by Cadena *et al.* (2020), *Stylemys nebrascensis* Leidy, 1851 by Ehret (2007), *Toxochelys latiremis* Cope, 1873 by Wilson (2023), and *Yaminuechelys maior* Staesche, 1929 by Pereyra *et al.* (2020). A comprehensive review of previous studies on turtle histology was finally recently presented by Scheyer & Cerda (2021). Overall, long bone histology and microarchitecture are probably the best documented for the marine turtle clade Chelonioidea Baur, 1893, but at least some visual documentation exists for a variety of other taxa (Table 1), which amounts to a relatively wide (although uneven and in some cases only cursory) sampling of recent taxa and very rudimentary exploration of fossil turtle limb histology. Works actually focused on long bone histology of fossil turtles are still rare (Ehret 2007; Danilov *et al.* 2018; Cadena *et al.* 2020; Pereyra *et al.* 2020; Sena *et al.* 2021; Bhat *et al.* 2023).

Likewise, although information on the correspondence between the body size, growth tempo, ecology, and limb bone histology in turtles improved in recent years, the sampling particularly for Mesozoic taxa is very poor (Pereyra *et al.* 2020; Sena *et al.* 2021; Wilson 2023), despite the potential usefulness of such data in evaluation of growth patterns, ecomorphology, and life strategies of extinct species. Though several studies explored the interplay between the preferred habitus and limb proportions in stem turtles (e.g. Joyce & Gauthier 2004; Lyson *et al.* 2016; Motani & Vermeij 2021; Dudgeon *et al.* 2021) and the ecology of the earliest stem-turtles is

TABLE 2. — Measured and estimated lengths of studied *Proterochersis porebensis* Szczygielski & Sulej, 2016 stylopodial bones.

Bone	Specimen number	Length as preserved (cm)	Estimated length (distal depth/length ratio) (cm)	Estimated length (extrapolation based on complete) (cm)	Used for
Humerus	ZPAL V. 39/50	10.6	10.6	–	CT
	ZPAL V. 39/156	7.7	7.6	–	CT
	ZPAL V. 39/433	3.8 (incomplete)	8.2	–	Histology
	ZPAL V. 39/439	2.2 (incomplete)	4.7	–	Histology
	ZPAL V. 39/446	5.8	5.9	–	CT
Femur	ZPAL V. 39/48	12.7	12.3	12.7	–
	ZPAL V. 39/432	14.0	14.5	14.0	CT
	ZPAL V. 39/499	2.7 (incomplete)	5.6	8.8	Histology
	ZPAL V. 39/500	6.6 (incomplete)	12.8	13.0	Histology

an eagerly discussed topic (e.g. Joyce & Gauthier 2004; Scheyer & Sander 2007; Li *et al.* 2008; Benson *et al.* 2011; Lyson *et al.* 2016; Lichtig & Lucas 2017; Lautenschlager *et al.* 2018; Bajdek *et al.* 2019; Schoch *et al.* 2019; Dziomber *et al.* 2020; Motani & Vermeij 2021; Dudgeon *et al.* 2021; Szczygielski & Słowiak 2022; Evers *et al.* 2022), relevant data for Triassic turtles are, in fact, still very scarce. Additionally, the poor understanding of the early turtle limb ontogeny and proportions makes it difficult to accurately evaluate the ontogenetic stage and estimate the total body size in case of isolated specimens. The life histories and growth strategies of Triassic turtles remain unexplored, especially that recent data (e.g. Joyce & Gauthier 2004; Scheyer & Sander 2007; Benson *et al.* 2011; Lichtig & Lucas 2017; Lautenschlager *et al.* 2018; Szczygielski *et al.* 2018; Bajdek *et al.* 2019; Dziomber *et al.* 2020; Dudgeon *et al.* 2021; Evers *et al.* 2022) have put aside or added nuance to the historical understanding of *Proterochersis* spp. as a small-bodied terrestrial form (Fraas 1913) and *Proganochelys quenstedtii* Baur, 1887 as a distinctly larger semiaquatic species (Fraas 1899; Gaffney 1990), suggesting instead that both genera could reach similar body sizes, *Proganochelys quenstedtii* was a terrestrial turtle, while at least *Proterochersis porebensis* Szczygielski & Sulej, 2016 was semiaquatic. The same problem, to a varied extent, applies also to more recent representatives of the group, especially considering for example their developmental plasticity.

Here, we present a histological description of the humeri and femora of *Proterochersis porebensis* from the Norian (Late Triassic) of Poręba, Poland (Sulej *et al.* 2012; Niedźwiedzki *et al.* 2014; Kubik *et al.* 2015; Szulc & Racki 2015; Szulc *et al.* 2015; Szczygielski & Sulej 2016; Bajdek *et al.* 2019) and a humerus of *Proganochelys quenstedtii* from the Norian (Late Triassic) of Frick, Switzerland (e.g. Braun 1920; Sander 1992; Jordan *et al.* 2016; Zahner & Brinkmann 2019; Scheyer *et al.* 2022). The Poręba assemblage is the only place known thus far to produce well-preserved long bones of proterochersids (thus far only a partial humerus and femur have been figured; Sulej *et al.* 2012; Szczygielski & Sulej 2016; comprehensive description in preparation). A second locality, Kocury, yielded only a very fragmentary femur (Czepiński *et al.* 2021). *Proterochersis porebensis* is among the oldest turtles presenting numerous plesiomorphic characters (e.g. Szczygielski & Sulej 2016, 2019; Szczygielski 2017; Sterli *et al.* 2021). *Proganochelys quenstedtii*, historically known only from Germany, is arguably the best-known stem turtle from the Late Triassic worldwide (e.g. Quenstedt 1889; Fraas 1899; Jaekel 1914, 1916; Ballerstedt 1922; Gaffney 1990; Joyce 2017; Scheyer *et al.* 2022; Werneburg *et al.* 2022). Limb bone histology of non-testudinate Pantestudines (Lyson *et al.* 2016; Schoch *et al.* 2019) and more derived turtles was studied in the past but no studies of Triassic turtle (Testudinata) limb histology were published to date (only singular CT slices of a humerus and femur of *Proganochelys quenstedtii* were presented thus far: Nakajima 2017; Schoch *et al.* 2019). This paper provides the first insight into the evolution of limb microstructure on the brink of the early testudinate radiation. Moreover, we evaluate the histological, morphometric, and morphological data in the context of growth patterns in Triassic stem turtles.

MATERIAL AND METHODS

PROTEROCHERSIS POREBENSIS

Eight specimens of *Proterochersis porebensis* were selected for study (Fig. 1A-P): two complete right humeri (ZPAL V. 39/50, Fig. 1I, J; ZPAL V. 39/156, Fig. 1E, F), one complete left humerus (ZPAL V. 39/446, Fig. 1C, D), distal parts of two right humeri (ZPAL V. 39/433, Fig. 1A, B; ZPAL V. 39/439, Fig. 1G, H), one complete right femur (ZPAL V. 39/432, Fig. 1O, P), and distal parts of two right femora (ZPAL V. 39/499, Fig. 1K, L; ZPAL V. 39/500, Fig. 1M, N). Although the selected specimens are isolated and some of them are fragmentary, they all originate from Poręba, Poland, the type locality of *Proterochersis porebensis*, which thus far has not produced any evidence of other turtle species (Sulej *et al.* 2012; Niedźwiedzki *et al.* 2014; Szczygielski & Sulej 2016, 2019; Szczygielski *et al.* 2018; Bajdek *et al.* 2019; Szczygielski & Słowiak 2022). Furthermore, the femora do not show morphological differences from the femur of the holotype (ZPAL V. 39/48) that could not be explained by ontogeny. The bones represent various size classes, from small, supposed juveniles (ZPAL V. 39/156, ZPAL V. 39/439, ZPAL V. 39/446, ZPAL V. 39/499 – individuals much smaller than the holotype, ZPAL V. 39/48, which is considered a sub-adult), through middle-sized (ZPAL V. 39/433 – about the size of the holotype), to large (ZPAL V. 39/432,

FIG. 1. — *Proterochersis porebensis* Szczygielski & Sulej, 2016, studied humeri (**A**-**J**) and femora (**K**-**P**), and the studied humerus of *Proganochelys quenstedtii* Baur, 1887 (**Q**, **R**) in dorsal (**A**, **C**, **E**, **G**, **I**, **K**, **M**, **O**, **Q**) and ventral (**B**, **D**, **F**, **H**, **J**, **L**, **N**, **P**, **R**) view: **A**, **B**, distal end of small right humerus ZPAL V. 39/439; **C**, **D**, small left humerus ZPAL V. 39/446; **E**, **F**, small right humerus ZPAL V. 39/156; **G**, **H**, distal end of middle-sized right humerus ZPAL V. 39/433; **I**, **J**, large right humerus ZPAL V. 39/50; **K**, **L**, distal end of small right femur ZPAL V. 39/499; **M**, **N**, distal end of large right femur ZPAL V. 39/500; **O**, **P**, large right femur ZPAL V. 39/432; **Q**, **R**, large left humerus SMF 09-F2. Sectioning planes for histology indicated in **red**. Scale bar: 1 cm.

ZPAL V. 39/500 – significantly larger than the holotype) and seemingly mature, as suggested by an advanced development of morphological characteristics (e.g. well-differentiated articular surfaces and processes, distal enclosure of the ectepicondylar foramen, pronounced muscle and tendon attachments). Note that these classes are approximate and introduced for convenience, since body size and proportions do vary between individuals of the same ontogenetic age (for discussion, see Szczygielski & Sulej 2016, 2019; Szczygielski *et al.* 2018; Szczygielski & Słowiak 2022).

The studied specimens, as well as the holotype femur (ZPAL V. 39/48), were measured and, in the case of incomplete material, their length was roughly estimated to better visualize their relative size (Table 2). Measurements included length, distal width (maximum width between the medial and lateral edges of the distal end), and distal depth (dorsoventral thickness of the distal end; see Appendix 1 for exact measurements). Surface area and volume were moreover calculated for complete femora (ZPAL V. 39/48 and ZPAL V. 39/432) based on 3D surface scans created using the Shining 3D EinScan Pro 2X 3D scanner fixed on a tripod with EinScan Pro 2X Color Pack (texture scans), Ein-Turntable (alignment based on features), and EXScan Pro 3.2.0.2-3.7.0.3 software, using the Compute Geometric Measures tool of MeshLab v. 2021.10 (Cignoni *et al.* 2008).

Basic statistics (standard deviation, mean, etc.) were calculated using Microsoft 365 Excel 64-bit v. 2301 (compilation 16.0.16026.20002). The linear correlation was calculated in PAST 4.03 (Hammer *et al.* 2001). Based on the measured relationship for complete humeri (ZPAL V. 39/50, ZPAL V. 39/156, ZPAL V. 39/446), the distal depth was found to be an adequate predictor of length (mean length to distal depth ratio = 5.87, standard deviation = 0.06, correlation r = 0.99, p = 0.01 vs mean length to distal width ratio = 2.46, standard deviation = 0.14, correlation r = 0.99, p = 0.06), allowing length estimation for ZPAL V. 39/433 and ZPAL V. 39/439. For femora, this relationship was less satisfactory (mean length to distal depth ratio = 5.58, standard deviation = 0.27 vs mean length to distal width ration = 2.91, standard deviation = 0.38). Because there are only two

complete femora (ZPAL V. 39/48 and ZPAL V. 39/432), neither of which are small, and possibly due to allometric increase in femur girth relative to length at more advanced ontogenetic stages (see below), calculations based on the mean ratio were found to underestimate the size of smaller femora and overestimate the size of large femora. For that reason, another method of estimation, based on extrapolation of growth trend delineated by ZPAL V. 39/48 and ZPAL V. 39/432, was attempted Appendix 2).

To calculate rough correspondence between the stylopodial bone and on carapace sizes in Triassic turtles, additional measurements of humeri (length, width of the head with shoulder), scapulocoracoids (maximum width of the coracoid facet of the glenoid), femora (length), and carapaces (midline carapace length) of *Proterochersis porebensis* ZPAL V. 39/48 and ZPAL V. 39/49, *Proganochelys quenstedtii* SMNS 16980, SMNS 17203, and SMNS 17204, as well as *Palaeochersis talampayensis* Rougier, Fuente & Arcucci, 1995 PULR 069 were obtained. These basic methods, clearly, only allow for limited accuracy and do not consider allometry or ontogenetic change of growth trajectory, but due to the very small sample size, they are deemed sufficient within the scope of the current work.

Fragmentary specimens (distal parts ZPAL V. 39/433, ZPAL V. 39/439, ZPAL V. 39/499, ZPAL V. 39/500) were cut transversely close to the mid-length. Although the sectioning plane is located below the center of ossification preserving the most complete record of growth (e.g. Balli 1937; Zug *et al.* 1986; Nakajima *et al.* 2014), skeletochronology is not the main objective of this work and, given the limited supply of *Proterochersis porebensis* limb bones and their preservation, we preferred to select a sectioning plane allowing observation of undamaged cortex and comparisons between specimens of varied sizes. Two adjacent thin sections were produced from the femur ZPAL V. 39/500 and the humerus ZPAL V. 39/439, and three for the humerus ZPAL V. 39/433. The thin sections were photographed using Nikon Eclipse LV100 POL polarizing microscope with a DS-Fil camera and Leica DM4 P polarizing microscope with a FLEXACAM C3 camera in transmitted normal and polarized light, including a quarter lambda plate. Composite pictures of whole sections were created using NIS-Elements 4.20.01 (for the Nikon microscope) microscope imaging software and Leica Application Suite X 5.1.0.25593 (for the Leica microscope). Measurements of cortical thickness were made using ImageJ 1.53e (Schneider *et al.* 2012).

Four complete specimens (ZPAL V. 39/50, ZPAL V. 39/156, ZPAL V. 39/432, ZPAL V. 39/446) were scanned with GE Phoenix v|tome|x microtomograph (Laboratory of Microtomography, University of Silesia), 1700 projections with 500 ms exposition time at 180 kV and 150 µA (ZPAL V. 39/50 and ZPAL V. 39/432) or 160 kV and 120 µA (ZPAL V. 39/156, ZPAL V. 39/446) with resolution of 40 µm (ZPAL V. 39/156 and ZPAL V. 39/446), 60 µm (ZPAL V. 39/50), or 75 µm (ZPAL V. 39/432). The CT data were subsequently reviewed and exported with Volume Graphics MyVGL 2022.2 (https://www.volumegraphics.com/). Slice sequences (see Appendices 1-16; and Morphosource) in uncompressed video format (MOV) were converted to MP4 to reduce file sizes using the open source video transcoder HandBrake (https://handbrake.fr/).

Proganochelys quenstedtii

One humerus of *Proganochelys quenstedtii* (15.63 cm long; Fig. 1Q, R; see Scheyer *et al.* 2022: fig. 13A-D) was sectioned petrographically at its proximal midshaft and scanned using a Nikon XTH 225 ST CT Scanner housed at the Anthropological Department of the University of Zurich, 3000 projections with 500 ms exposition time at 174 kV and 435 µA, and resolution of 80 µm. The humerus belongs to a fairly complete specimen (SMF 09-F2) from the Frickberg (Norian) close to the village of Frick, Switzerland (Scheyer *et al.* 2022). Prior to sectioning with a diamond-sintered blade mounted on a Buehler IsoMet low speed precision saw, the shaft of the humerus was stabilised using Technovit 5071 (two component resin on methyl-methacrylate basis). Sections were then glued to a glass object slide and ground down to 60-80 microns in thickness, before being studied under normal transmitted and cross-polarized light using a Leica DM 2500 M composite microscope equipped with a Leica DFC 420 C digital camera. Final processing of the CT data (contrast balancing, export of slices along particular planes) was performed in 3D Slicer 5.2.1 (https://www.slicer.org; Fedorov *et al.* 2012; Kikinis *et al.* 2014).

Abbreviations

Institutions

PULR Universidad Nacional de La Rioja, La Rioja;
SMF Sauriermuseum Frick, Frick;
SMNS Staatliches Museum für Naturkunde Stuttgart, Stuttgart;
ZPAL Institute of Paleobiology, Polish Academy of Sciences, Warsaw.

Others

EFS external fundamental system;
MaCL maximum carapace length;
MiCL midline carapace length;
OCL outer circumferential layer.

RESULTS

Long bone microanatomy and bone histology of *Proterochersis porebensis*

All sectioned bones of *Proterochersis porebensis* present a well-developed, compact cortex and medullary area filled with cancellous bone (Fig. 2A-I). Thickness of the cortices (without erosion cavities and remodeling) is 2.2-3.4 mm, and 1.2-1.7 mm for the middle-sized and small humerus specimen and 0.7-2.4 mm and 0.7-1.3 mm for the large and small femora, respectively. The matrix of the cortex is composed predominantly of parallel-fibered bone (Figs 2A-I; 3A-D; 4A-F; 5; 6) that often shows high organization (approaching

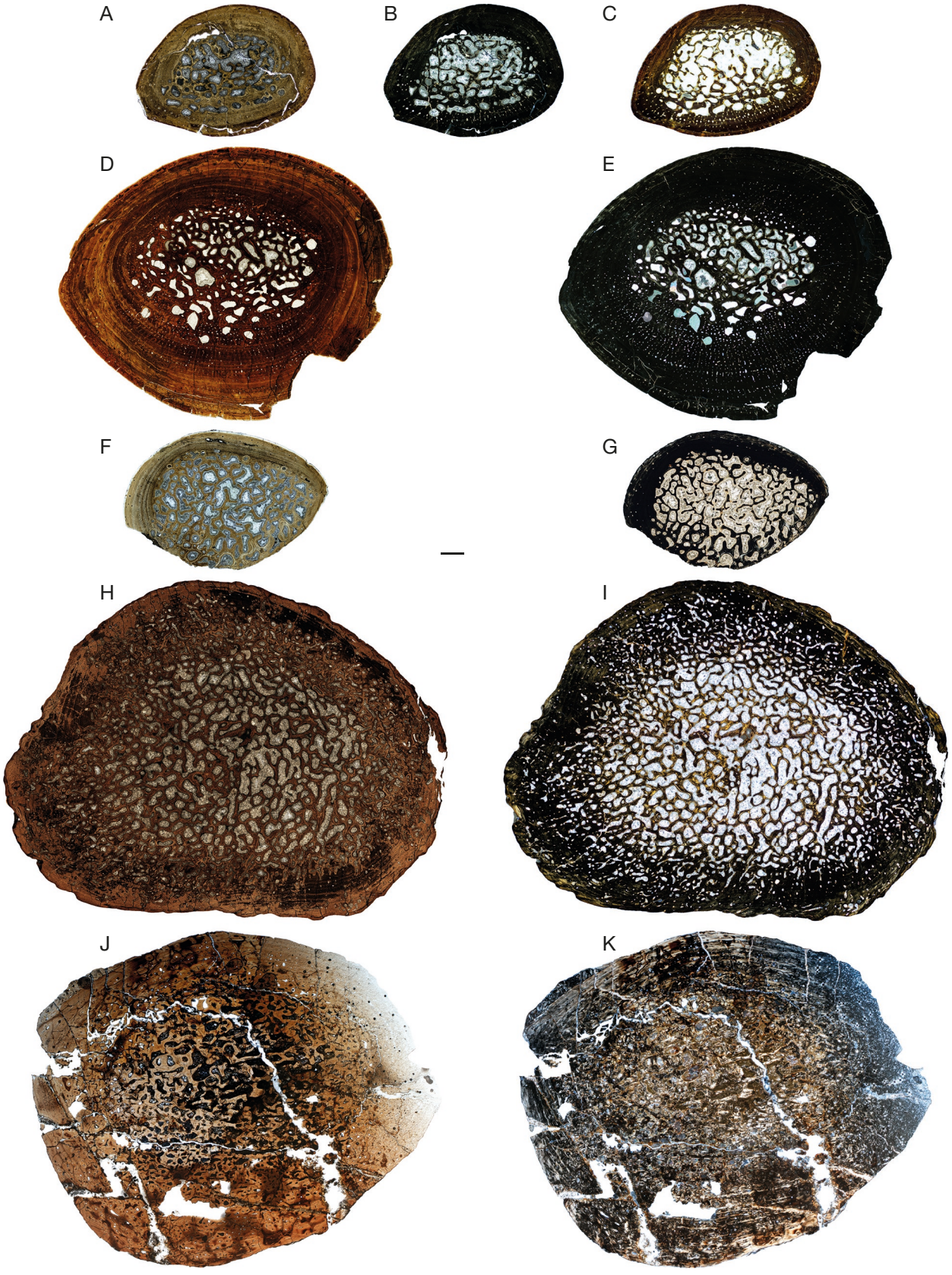

FIG. 2. — *Proterochersis porebensis* Szczygielski & Sulej, 2016 (**A**-**I**) and *Proganochelys quenstedtii* Baur, 1887 (**J**, **K**), thin sections in normal transmitted (**A**, **D**, **F**, **H**, **J**), polarized (**B**, **E**, **G**, **I**, **K**), and polarized with quarter lambda plate I (**C**) light: **A**-**E**, right humeri: **A**-**C**, small ZPAL V. 39/439; **D**, **E**, middle-sized ZPAL V. 39/433; **C** adjacent (slightly more distal) to **A** and **B**; **F**-**I**, right femora: **F**, **G**, small ZPAL V. 39/499; **H**, **I**, large ZPAL V. 39/500; **J**, **K**, left humerus, large SMF 09-F2. Dorsal surface towards the top of the page, anterior surface to the left. Scale bar: 1 cm.

but not exactly the same as the lamellar bone in the same sections) and is even locally grading into lamellar bone in some samples, and in the middle-sized humerus ZPAL V. 39/433 (Fig. 4B) and large femur ZPAL V. 39/500 (Fig. 6D) it locally takes a highly organized appearance, approaching lamellar bone. The matrix shows annular (ring-like) lines of arrested growth (LAGs), which appear relatively even in the small femur ZPAL V. 39/499 (Figs 2F; 5A) and in the deeper part of the cortex of the small humerus ZPAL V. 39/439 (Figs 2A; 3C, E), but show more pronounced waviness in the external part of the cortex of ZPAL V. 39/439 (Figs 2A; 3C) and in the larger ZPAL V. 39/433 (Figs 2D; 4A, E) and ZPAL V. 39/500 (Figs 2H; 6E). The vascularization in the cortex is generally poor, especially in the external layers, although some local variability is visible along the perimeter of the bones (e.g. the cortex of the humeri is clearly more vascularized ventrally than dorsally; Figs 2A-E; 3A-D; 4A-F). The vascularization pattern is sub-longitudinal, arranged in circular patterns, with slight radial inclination visible in all specimens except ZPAL V. 39/499 (small femur). The vasculature in most sectioned bones is predominantly primary (primary canals without primary osteons and, locally, osteons). The incipient secondary remodeling (sparsely scattered secondary osteons, Fig. 4E) is present in the middle-sized humerus ZPAL V. 39/433. Only in the large femur ZPAL V. 39/500 is the secondary remodeling significant and, in some places, nearly reaches the external surface, although much of the primary tissue and some primary vascular canals are still locally present (Fig. 6). The small femur ZPAL V. 39/499 retains mostly non-remodeled cortex, but evidence of active remodeling is visible at the border between the cortex and the medullary region, where two to three overlapping generations of lamellar bone are present (Fig. 5). The large femur ZPAL V. 39/500 differs from the other sampled bones in having a clearly scalloped external surface due to a network of vascular grooves, which is visible also macroscopically (Figs 1M, N; 2H, I; 6). These grooves seem to be mostly imprints of superficial vasculature, but numerous vascular openings are also present on the dorsoposterior surface of the distal expansion of that specimen.

The extent of the cancellous area appears to be smaller in the humeri than in the femora and more clearly defined in the small than in the middle-sized and large specimens (Fig. 2A-I). The trabeculae partly retain primary tissue in interstitial spaces, which are lined by endosteal lamellar bone, especially close to the cortex, and even in the smallest sampled specimens clearly incorporate periosteal tissue (Figs 2A-I; 3; 4C, D; 5; 6). Especially in the large femur ZPAL V. 39/500, the boundary between the endosteal cancellous and periosteal cortical region is gradual, with large areas of the periosteal cortex remodeled into either intertrabecular spaces or irregularly meandering secondary osteons (Figs 2H, I; 6). In the same specimen, trabeculae deeper inside the bone are comparatively very thin. The thickness and length of the trabeculae is, nonetheless, varied; they appear more slender and longer in the central and dorsal part of the medullary area (Fig. 2A-I), but some regions of increased thickness are locally evident, especially in the middle-sized humerus ZPAL V. 39/433 (Figs 2D, E; 4G, H).

The CT data (Fig. 7) illustrate a gradual ontogenetic progression of the trends observed in the histological sections and reveal the microstructural patterns along the bone length. Both the absolute and relative thickness of the cortices appears to increase with increasing bone size. In that regard, ZPAL V. 39/446 (cortex 1.6-2.16 mm) and ZPAL V. 39/156 (cortex 1.9-2.3 mm), which are intermediate in size between the sectioned ZPAL V. 39/439 and ZPAL V. 39/433, are also intermediate structurally – their cortices are thicker than in ZPAL V. 39/439 (1.2-1.7 mm), but thinner than in ZPAL V. 39/433 (2.2-3.4 mm; note that the cortical thickness in sectioned specimens is undervalued due to the slightly more distal plane of sectioning). The large humerus (ZPAL V. 39/50, cortex 2.8-3.4 mm) and femur (ZPAL V. 39/432, cortex 3.2-4 mm, compared to 0.7-1.3 mm in ZPAL V. 39/499 and 2-2.4 mm in ZPAL V. 39.500) generally follow the trends of cortical thickening with increasing size suggested by the smaller specimens.

As indicated by previous studies, the centers of ossification are located slightly more proximally than the midshaft and are associated with the largest thickness of the cortices (Fig. 7A, C, E, G). In small humeri, the cortices in that region are relatively compact (in ZPAL V. 39/446 more so than in ZPAL V. 39/156) and the trabecular bone in the bone center has a relatively uniform structure (Fig. 7A-D) probably indicating low remodeling (although potentially also dependent on stress distribution patterns and load). In ZPAL V. 39/50, however, the cortex is somewhat more vascularized (although still relatively poorly), but the interior trabecular region is much less defined and denser than in smaller specimens, indicating more pronounced remodeling (Fig. 7E, F). There is no central marrow cavity in the studied humeri. Conversely, in the large femur ZPAL V. 39/432, the internal trabecular region is still distinct (even though it is denser than in the areas further away from the ossification center) and there is a small, irregular region devoid of trabeculae located around the level of the ossification center (Fig. 7G, H). This cavity is connected with the bone exterior via two well-defined nutrient canals extending: 1) dorsoproximoanteriorly and eventually opening as a nutrient foramen at the anterodorsal base of the trochanter major; and 2) ventrodistally and opening as a nutrient foramen in the popliteal fossa, between the tibial and fibular condyle (see Appendices 1-16; and Morphosource).

Proximally and distally from the centers of ossification, the thickness of the cortex steadily decreases so in the areas of the proximal and distal articular surfaces the trabeculae nearly reach the bone exterior (Fig. 7A, C, E, G). The cortex, however, retains a relatively constant thickness across the intertubercular fossa of the humeri (Fig. 7A, C; Appendices 1-16; and Morphosource). In ZPAL V. 39/446 in that area it is perforated by numerous vascular canals roughly parallel to the long axis of the bone (Fig. 7A).

Trabeculae are relatively long and thick in the small humerus ZPAL V. 39/446 (Fig. 7A). In the slightly larger ZPAL V. 39/156 they retain a similar morphology close to the cortex (especially ventrally) and around the level of the center of ossification, but become finer and more densely packed in the middle of the more proximal and distal portions

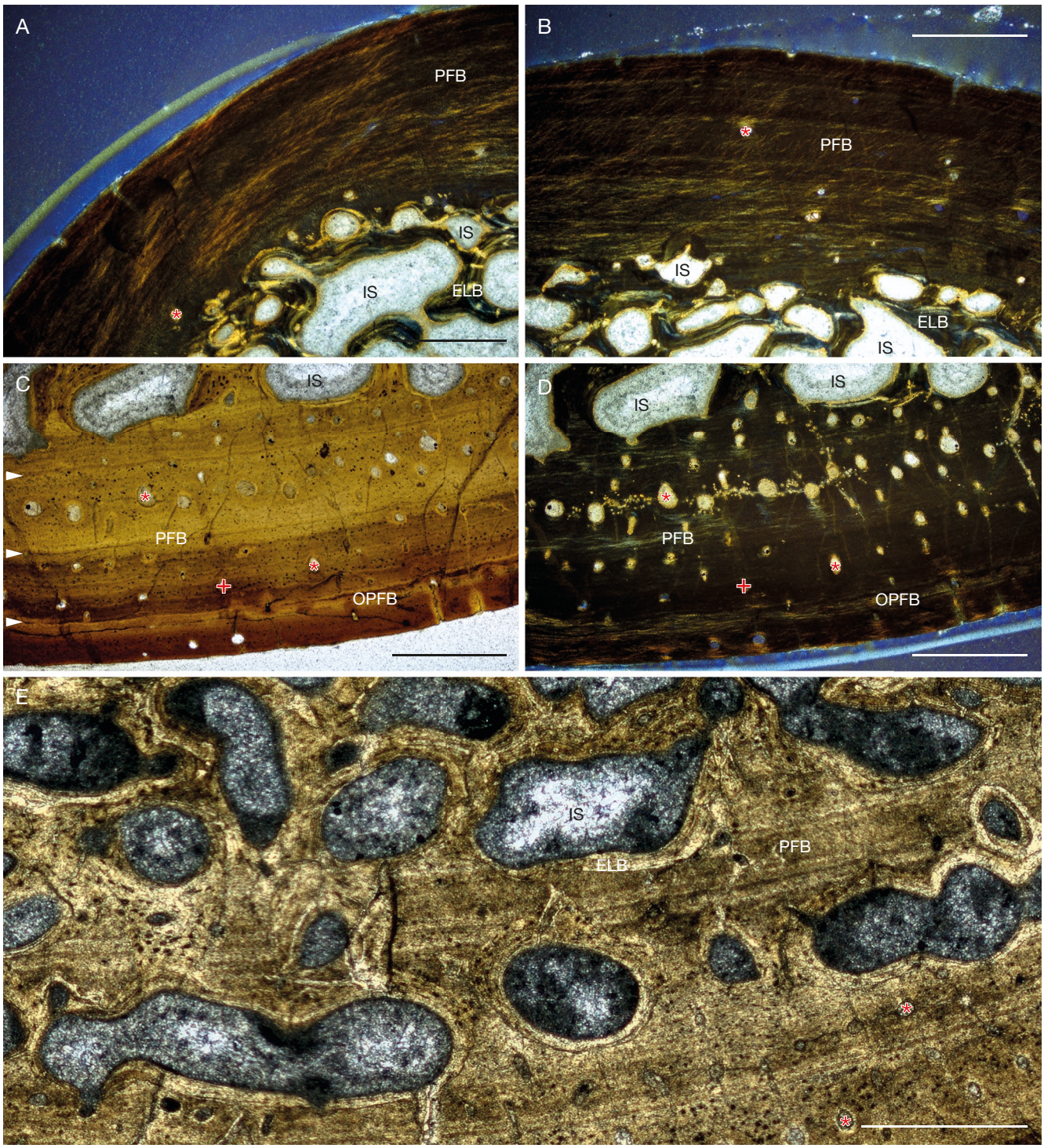

FIG. 3. — *Proterochersis porebensis* Szczygielski & Sulej, 2016, thin sections of small right humerus ZPAL V. 39/439: **A**, anterodorsal region showing relatively thin, nearly avascular cortex composed of parallel-fibered bone with gently undulating collagen fibers and thin trabeculae composed mostly of endosteal lamellar bone; **B**, dorsal region showing undulating collagen fiber layout parallel to bone surface and sparse collagen fibers oblique to the bone surface in the cortex, slightly increased longitudinal primary vasculature, and trabeculae incorporating cortical parallel-fibered bone; **C**, **D**, ventral region showing more developed vasculature (mostly primary canals with sporadic primary osteons, predominantly longitudinal), growth marks, and parallel-fibered matrix grading externally into more ordered, nearly lamellar bone; **E**, border between the cortex and the medullary region in the ventral part of the bone, adjacent (slightly more proximally) to **A**-**C** showing a large chunk of cortical parallel-fibered bone incorporated into the medullary region. **A**, **B**, **D** in polarized light with quarter lambda plate, **C** and **E** in normal transmitted light. Abbreviations and symbols: **ELB**, endosteal lamellar bone; **IS**, intertrabecular space; **PFB**, parallel-fibered bone; **OPFB**, higher organization of parallel-fibered bone; *, primary vascular canal; **red +**, primary osteon. Lines of arrested growth (LAGs) indicated with **arrowheads**. Scale bars: 500 µm.

TABLE 3. — Carapace, humerus, and femur measurements and length ratios in *Proganochelys quenstedtii* Baur, 1887, *Proterochersis porebensis* Szczygielski & Sulej, 2016, and *Palaeochersis talampayensis* Rougier, Fuente & Arcucci, 1995. Carapace length estimation for SMNS 17203 taken from Gaffney (1990). Abbreviations: **R**, right; **L**, left; *, preservation (e.g. damage or deformation) possibly affecting length and resulting ratios.

Species	Specimen	Midline carapace length (cm)	Humerus length (cm)	Humerus/carapace length ratio	Femur length (cm)	Femur/carapace length ratio	Humerus/femur length ratio
Palaeochersis talampayensis	PULR 068	45.5	L: 12.7 R: 12.0	L: 0.28 R: 0.26	L: 11.9 R: 11.6	L: 0.26 R: 0.25	L: 1.07 R: 1.03
Proganochelys quenstedtii	SMNS 16980	48.5	L: 13.4 R: 13.9	L: 0.28 R: 0.29	L: 15.3 R: 15.7*	L: 0.32 R: 0.32*	L: 0.88 R: 0.89*
	SMNS 17203	40* (estimated)	L: 9.8* –	L: 0.25* –	L: 13.1 R: 14.4*	L: 0.32* R: 0.36*	L: 0.75* –
	SMNS 17204	≥ 50*	– R: > 13*	– R: > 0.26*	L: 15.8 R: 15.9	L: 0.32 R: 0.32	> 0.82* –
	SMF 09-F2	55	L: 15.6	L: 0.28	–	–	–
Proterochersis porebensis	ZPAL V. 39/48	39.5	–	–	R: 12.7	R: 0.32	–

of the bone (Fig. 7C). In the large humerus ZPAL V. 39/50, they are generally more irregular, with larger and smaller intertrabecular spaces and thinner and thicker trabeculae scattered without a clear pattern (Fig. 7E). In the large femur ZPAL V. 39/432, the pattern of longer trabeculae closer to the cortex and finer trabeculae more interiorly is also noticeable, but less clear than in the humeri (Fig. 7G).

Overall, based on the histological sections and CT images, the humeri appear denser than the femora of comparable ontogenetic stages.

HUMERAL HISTOLOGY OF *PROGANOCHELYS QUENSTEDTII*

Most of the humeral cross section of SMF 09-F2 (about 77% of the lateromedial diameter) is formed by a spongious inner medullary region (Fig. 2J, K), which is typical for all turtles and independent of their respective life style (e.g. Nakajima *et al.* 2014). The cortical thickness varies between approximately 1.8 mm and 3 mm. The "pure" cortex (i.e., without any erosion or remodeling) is difficult to measure due to scattered erosion cavities and secondary osteons (see below). The medullary region consists of endosteal bone and irregularly formed medium-sized and small erosion cavities (Figs 2J, K; 8G, H). The medullary region grades into a perimedullary region (Figs 2J, K; 8C-F) where erosion cavities and endosteal bone are intermixed or grade into, respectively, large secondary osteons. Smaller scattered secondary osteons reach far into the outer cortex. Only the outer third of the cross section displays primary cortex (Figs 2J, K; 8A-F). This periosteal tissue consists generally of in overall low vascularized parallel-fibered tissue, locally even grading into lamellar tissue. The inner preserved cortex is subsequently followed or partially intermixed with the perimedullary region. It shows less organized and less strongly vascularized parallel-fibered tissue. Small longitudinal and few reticular to radial simple vascular canals, as well as some longitudinal primary osteons occur, which are not ordered in a clear pattern. The number of osteocyte lacunae is low and they remain small and flattened throughout. At the dorsolateral bone side, the highly organized, poorly vascularized outer cortex is followed by local regions of less organized parallel-fibered tissue, indicating an area of temporary faster growth (Fig. 8A, B). This area is barely recognizable as a slight rugosity on the bone surface. It likely represents a kind of localized pathology, potentially a small surface exostosis (Rothschild *et al.* 2012). The outer cortex contains 6-7 growth marks, indicated by thin annuli in the inner cortex and LAGs (lines of arrested growth) or multiple closely spaced rest lines in the outermost cortex. This resembles, at least locally, an outer circumferential layer (OCL)/external fundamental system (EFS; Ponton *et al.* 2004), but is not deposited all around the outermost cortex of the cross section. Growth marks in the inner cortex, which would represent earlier ontogenetic stages, are already lost due to remodeling. Extensive secondary remodeling is also revealed along the bone, including the area of the ossification center, by CT data (Fig. 7I, J). There is no medullary cavity proximal or distal to the thin-sectioning plane. Based on the increase in tissue organization and the nearly avascular condition and increase of the number of growth marks in the outer cortex, growth rate was clearly reduced, and the specimen likely represents an adult individual close to or already fully-grown. This late ontogenetic stage of SMF 09-F2 is also supported by humerus and carapace lengths that are in the upper range of other known individuals of *Proganochelys quenstedtii* (Gaffney 1990; Scheyer *et al.* 2022).

LIMB-BODY SIZE-ONTOGENETIC STAGE CORRESPONDENCE IN TRIASSIC TURTLES

Whereas comparisons between bones within one species are relatively easy and approximate ontogenetic stages can be established based on size and degree of ossification, interspecific comparisons require some additional discussion. Ratios between stylopodial bone and shell lengths in Triassic turtles is in some cases difficult to establish due to limited sample size and poor preservation (damage, deformation, etc.), but they apparently vary between taxa (Table 3).

Proganochelys quenstedtii provides the best insight, because its hypodigm includes associated sub-complete limbs and shells of four specimens of varied sizes, although their preservation in some cases makes precise measurements difficult: in SMNS 16980, the distal part of the right femur is damaged;

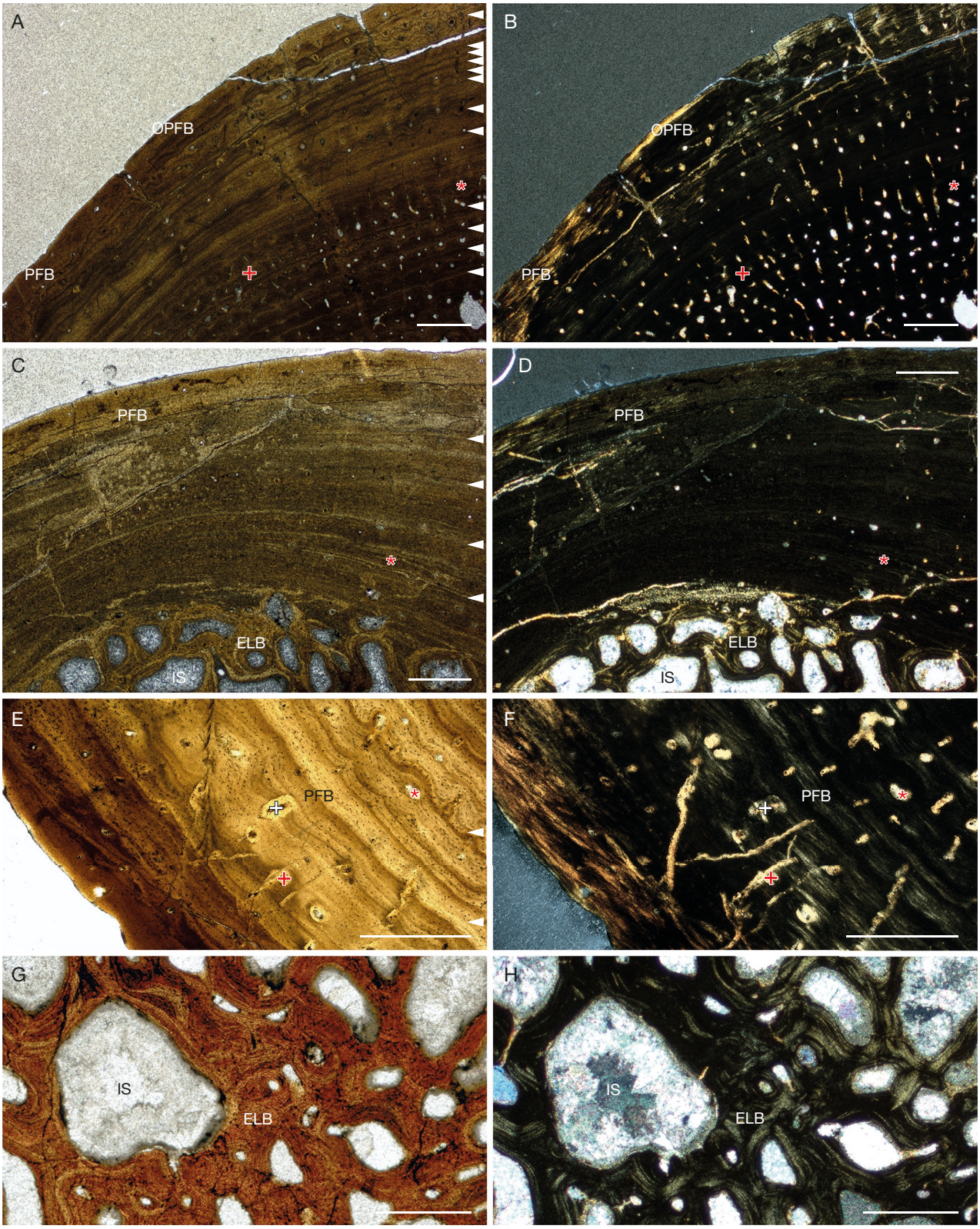

FIG. 4. — *Proterochersis porebensis* Szczygielski & Sulej, 2016, thin sections of middle-sized right humerus ZPAL V. 39/433: **A**, **B**, anterodorsal region showing predominantly parallel-fibered bone matrix externally grading into higher organized, nearly lamellar bone with primary vasculature (richer in the deeper cortex than externally, longitudinal to radial) and undulating LAGs; **C**, **D**, dorsal region with sparse primary longitudinal vasculature and trabeculae incorporating cortical parallel-fibered tissue; **E**, **F**, anteroventral region showing coarse collagen bundles in the parallel-fibered matrix, longitudinal to radial predominantly primary vasculature with sparse secondary osteons, and undulating LAGs; **G**, **H**, interior of the medullary region presenting thick trabeculae composed of endosteal lamellar bone. **A**, **C**, **E**, **G** in normal transmitted light, **B**, **D**, **F**, **H** in polarized light. Abbreviations and symbols: **ELB**, endosteal lamellar bone; **IS**, intertrabecular space; **PFB**, parallel-fibered bone; **OPFB**, higher organization of parallel-fibered bone; *, primary vascular canal; **red +**, primary osteon; **black and white +**, secondary osteon. Lines of arrested growth (LAGs) indicated with **arrowheads**. Scale bars: 500 µm.

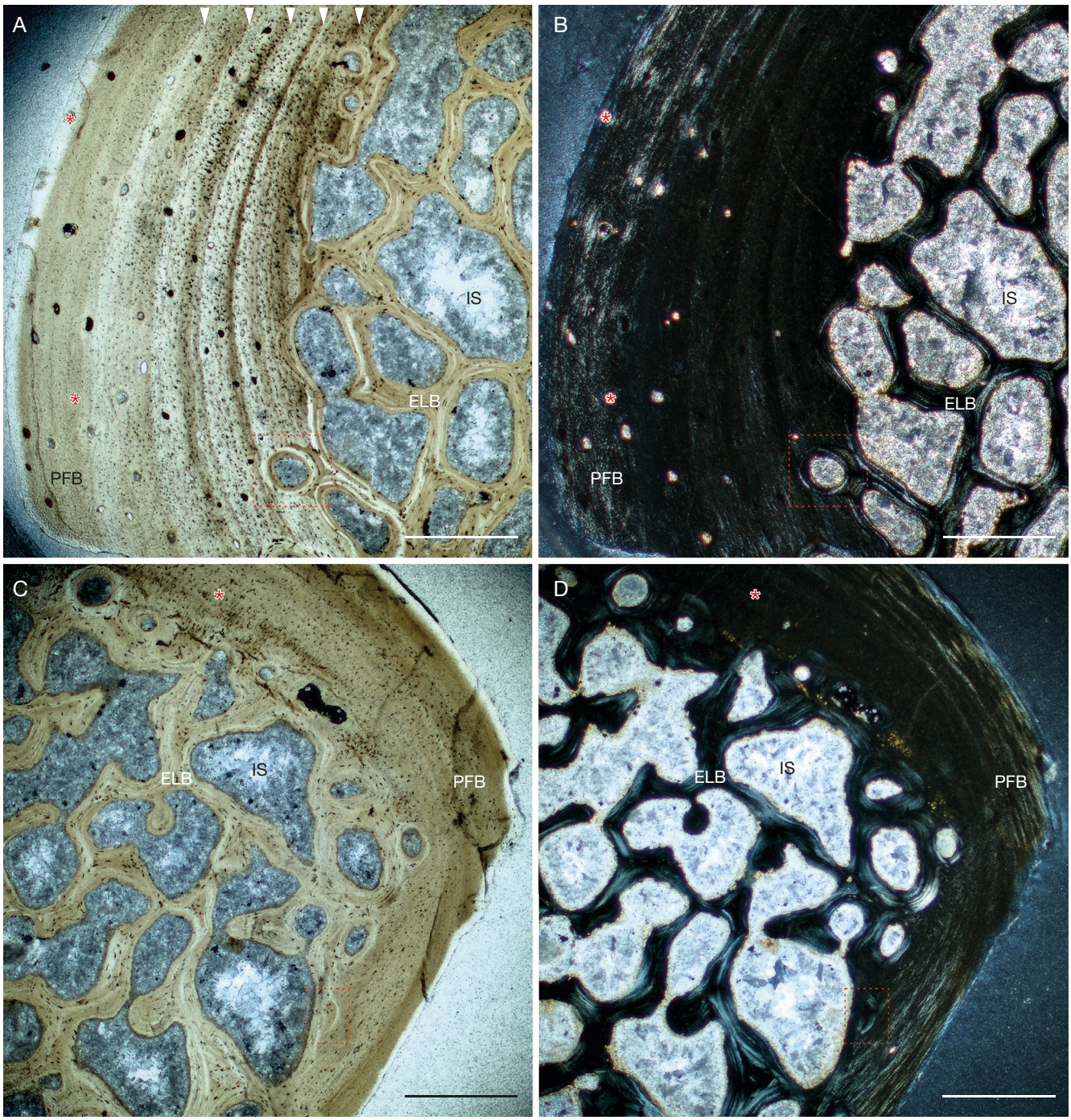

Fig. 5. — *Proterochersis porebensis* Szczygielski & Sulej, 2016, thin sections of small right femur ZPAL V. 39/499: **A**, **B**, anterior region showing parallel-fibered matrix with longitudinal primary canals and straight LAGs; **C**, **D**, posterior region with thinner and less vascularized cortex (note that the external cortex is destroyed posteroventrally) and indistinct growth marks. Despite the small size of the specimen and primary nature of the cortical tissue, the boundary between the cortex and medullary region reveals active remodeling evidenced by two to three generations of secondary lamellar bone (marked with red rectangles). **A** and **C** in normal transmitted light, **B** and **D** in polarized light. Abbreviations and symbols: **ELB**, endosteal lamellar bone; **IS**, intertrabecular space; **PFB**, parallel-fibered bone; *, primary vascular canal. Lines of arrested growth (LAGs) indicated with **arrowheads**. Scale bars: 500 µm.

in SMNS 17203, nearly no dermal rim of the carapace is preserved, the distal end of the left (only) humerus is damaged, and the right femur is flattened; and in SMNS 17204 the carapace is damaged and the proximal end of the right (only) humerus is obscured by rock matrix. Limb bones of SMF 09-F2 are compacted, but this likely has no significant effect on the length of the humerus. Accounting for those factors, the humerus to midline carapace length ratio in that species is about 0.28 (non-significant positive correlation: $y = 1.063\ x - 0.657$; $r = 0.97$; $p > 0.1$), the femur to midline carapace length ratio is about 0.32 (quite consistently; significant negative correlation $y = 0.85\ x - 0.24$; $r = 0.99$; $p < 0.01$), and the humerus is slightly shorter than the femur. Interestingly, in the smallest and morphologically most juvenile specimen, SMNS 17203,

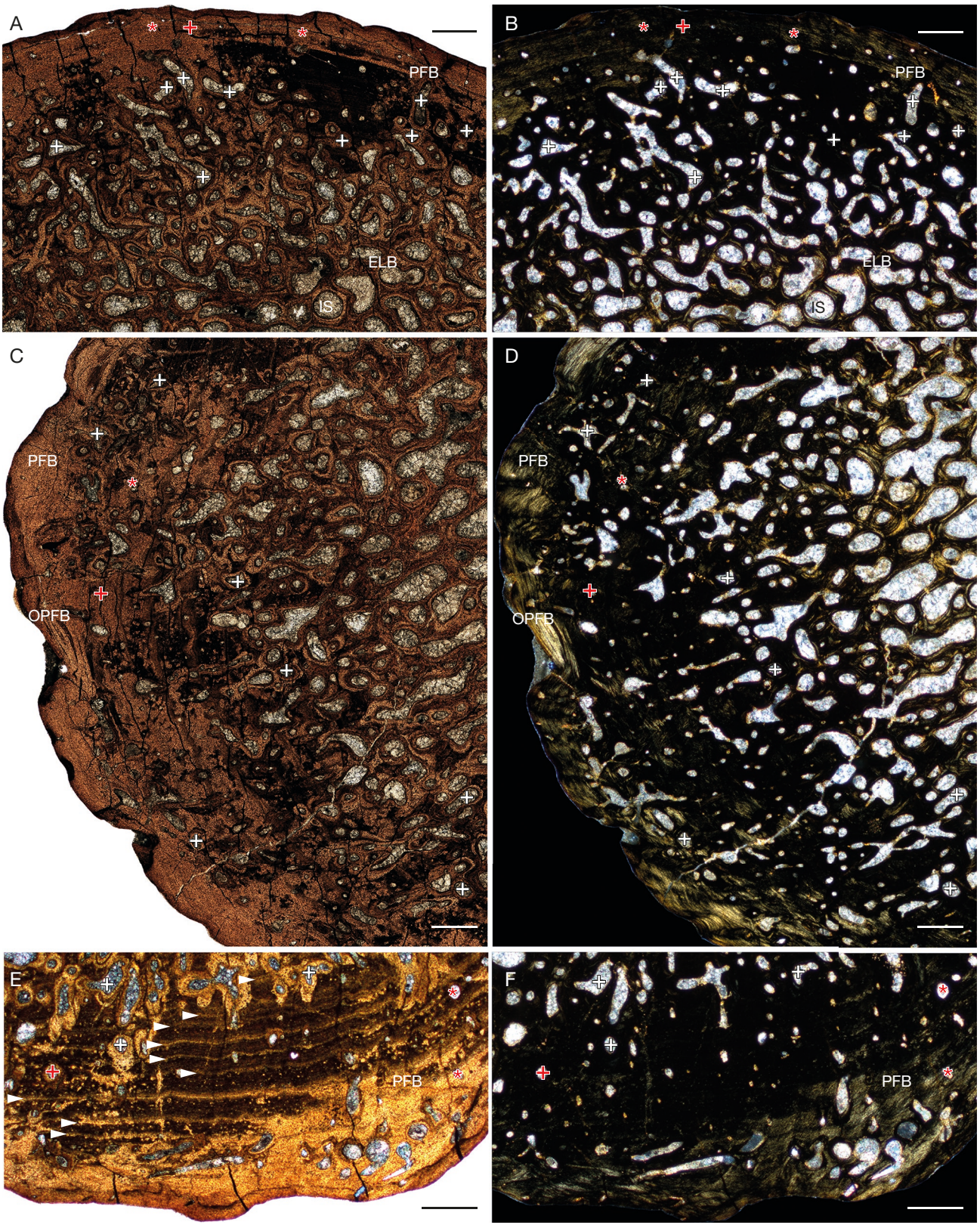

FIG. 6. — *Proterochersis porebensis* Szczygielski & Sulej, 2016, thin sections of large right femur ZPAL V. 39/500: **A**, **B**, dorsal region showing predominantly parallel-fibered bone matrix with longitudinal primary canals in the external part, numerous large, meandering secondary osteons in the deeper cortex, and gradual gradation into the medullary region; **C**, **D**, anterior region with parallel-fibered bone locally grading into higher organized, nearly lamellar bone; **E**, **F**, posteroventral region locally showing slightly less intensive invasion of remodeling, preserving undulating LAGs. Note the scalloped external surface. **A**, **C**, **E** in normal transmitted light, **B**, **D**, **F** in polarized light. Abbreviations and symbols: **ELB**, endosteal lamellar bone; **IS**, intertrabecular space; **PFB**, parallel-fibered bone; **OPFB**, higher organization of parallel-fibered bone; *****, primary vascular canal; **red +**, primary osteon; **black and white +**, secondary osteon. Lines of arrested growth (LAGs) indicated with **arrowheads**. Scale bars: 500 µm.

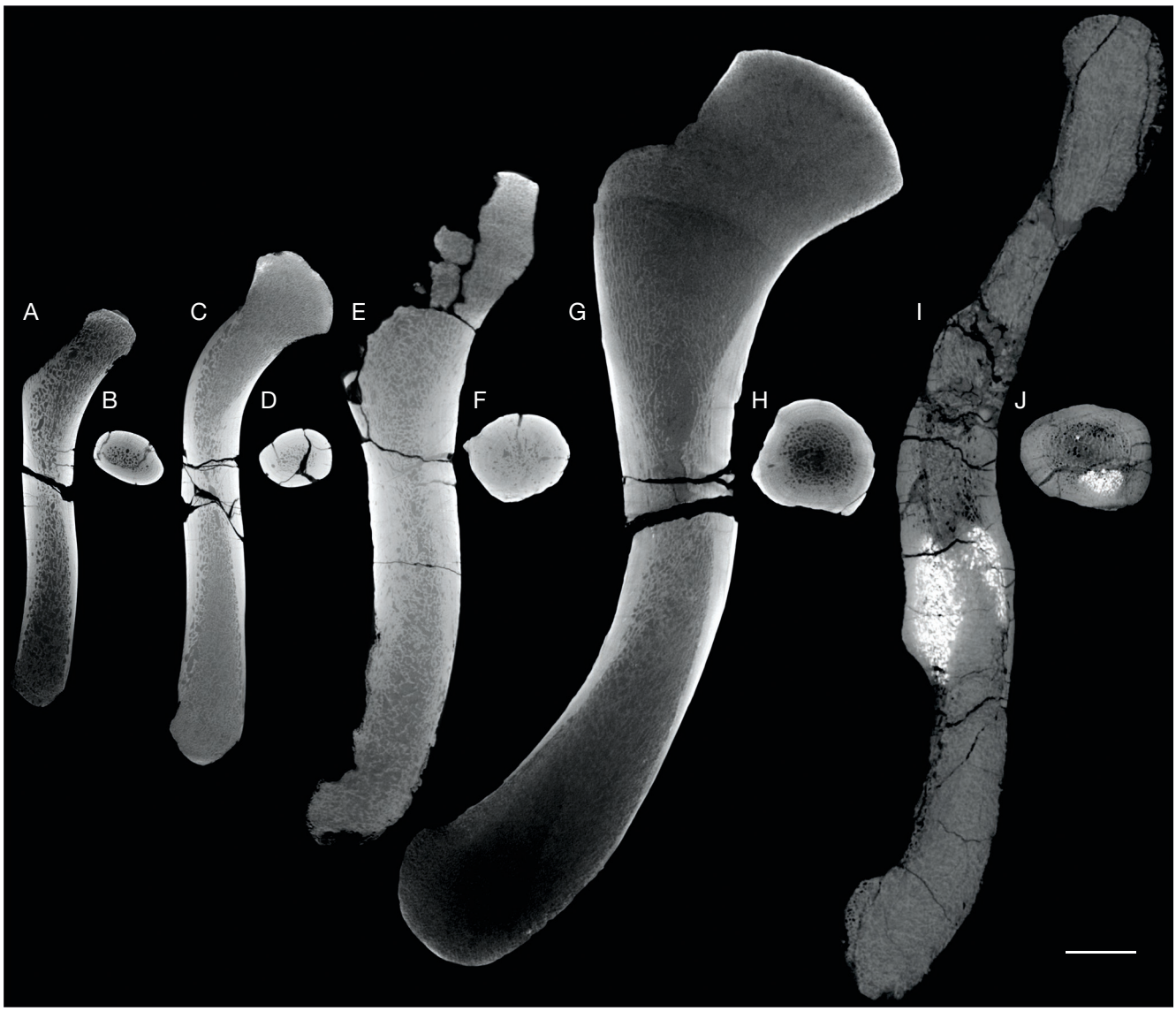

Fig. 7. — CT slices of humeri (**A**-**F**) and femur (**G**, **H**) of *Proterochersis porebensis* Szczygielski & Sulej, 2016 and humerus of *Proganochelys quenstedtii* Baur, 1887 (**I**-**J**), sagittal (**A**, **C**, **E**, **G**, **I**), and transverse at the level of the ossification center or as close as possible allowed by specimen preservation (**B**, **D**, **F**, **H**, **J**): **A**, **B**, small left humerus ZPAL V. 39/446; **C**, **D**, small right humerus ZPAL V. 39/156; **E**, **F**, large right humerus ZPAL V. 39/50; **G**, **H**, large right femur ZPAL V. 39/432; **I**, **J**, large left humerus SMF 09-F2. Dorsal surface to the right for **A**, **C**, **E**, **G**, **I** and towards the top of the page for **B**, **D**, **F**, **H**, **J**. Scale bar: 1 cm.

the humerus is quite clearly proportionally smaller than in larger specimens, even considering its damaged distal part. This suggests that the limbs could exhibit some allometry. The midline carapace length (MiCL) in known specimens of *Proganochelys quenstedtii* spans between about 40 cm in the presumed juvenile SMNS 17203 (estimated by Gaffney 1985, 1990), through 48.5 cm in SMNS 16980 considered a subadult (Gaffney 1990), to 60 cm in presumably adult SMNS 10012 (Gaffney 1985, 1990). SMF 09-F2 is almost as large, measuring 55 cm of MiCL (Scheyer *et al.* 2022).

In *Palaeochersis talampayensis* holotype (PULR 068), the humerus to carapace length ratio is nearly the same as in *Proganochelys quenstedtii* (average based on the left and right humerus = 0.27). However, the femur is proportionally shorter (femur to carapace length ratio about 0.26, humerus to femur length ratio about 1.05). Since only one published individual of that species preserves shell and stylopodial bones (Rougier *et al.* 1995; Sterli *et al.* 2007), it is not possible to estimate the size range, however, the bones appear well-ossified, suggesting an advanced ontogenetic stage.

The only individual of *Proterochersis porebensis* preserving both the shell and the femur is the holotype, ZPAL V. 39/48, a presumed subadult (Szczygielski & Sulej 2016). The MiCL in that specimen is 39.5 cm (42.5 cm of maximum carapace length [MaCL]) and the femur is 12.7 cm long. This results in a femur to MiCL ratio of 0.32, the same as in *Proganochelys quenstedtii*. The largest complete shell of *Proterochersis porebensis* recovered thus far is ZPAL V. 39/49 (MaCL = 49 cm, MiCL = 44.5 cm), but the maximum carapace length for the species, based on fragmentary remains of a large individual (ZPAL V. 39/60), was estimated to be about 60 cm (Szczygielski *et al.* 2018). Based on the average carapace measurements of

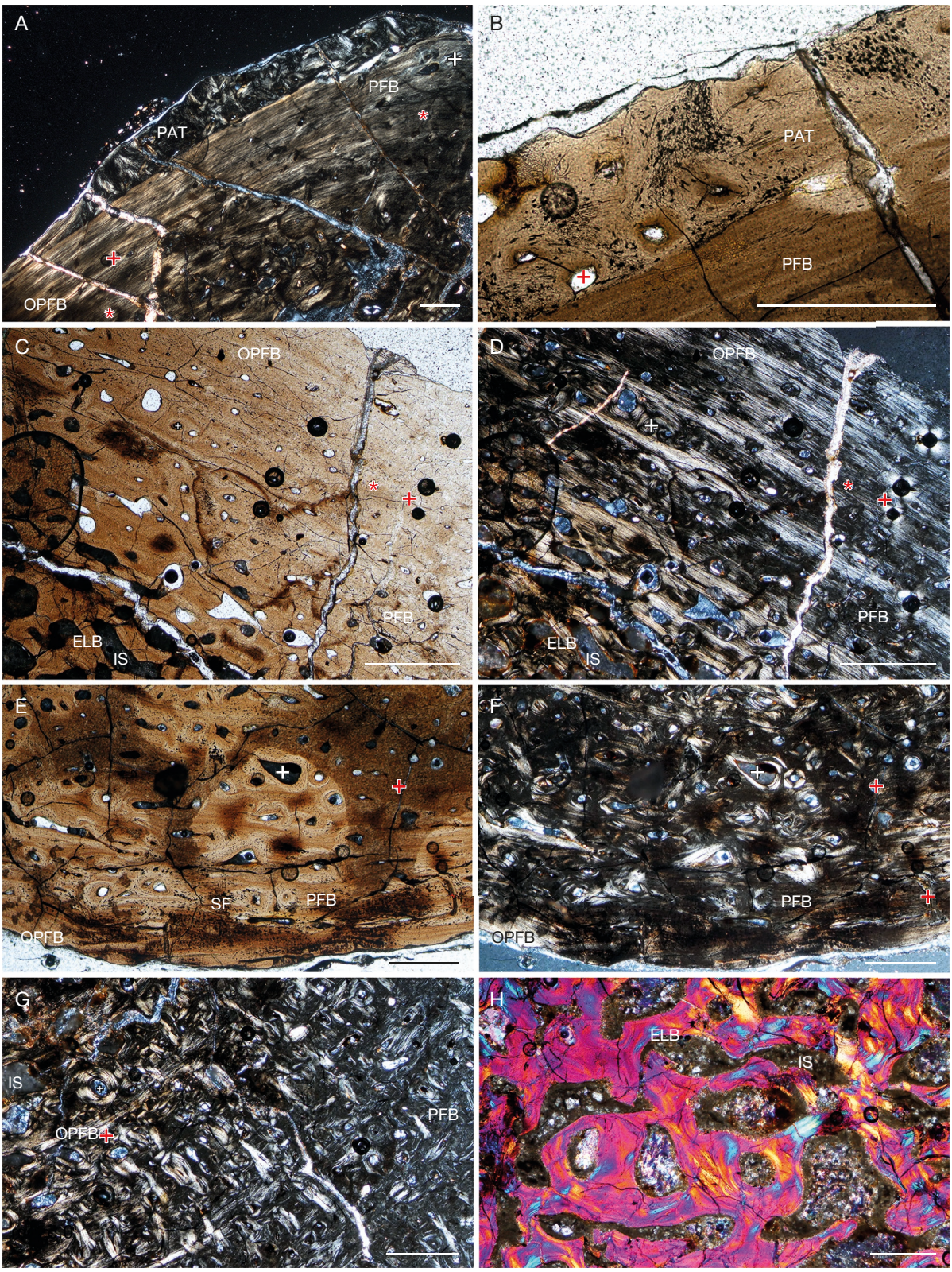

FIG. 8. — *Proganochelys quenstedtii* Baur, 1887, thin sections of large left humerus SMF 09-F2: **A**, anterodorsal region showing predominantly parallel-fibered bone matrix with predominantly longitudinal primary canals and primary osteons and pathological exostosis; **B**, closeup of the pathology, showing osteocyte lacunae aggregations; **C**, **D**, posterodorsal region with parallel-fibered bone locally grading into higher organized, nearly lamellar bone, secondary remodeling and gradual gradation into the medullary region; **E**, **F**, ventral region locally showing more intensive remodeling and Sharpey's fibers; **G**, posteroventral region showing intensive remodeling of the deeper cortex and numerous radially inclined primary and secondary osteons, **H**, interior of the medullary region presenting thick trabeculae composed of endosteal lamellar bone. **A**, **D**, **F**, **G** in polarized light, **B**, **C**, **E** in normal transmitted light, **H** in polarized light with 530 nm λ plate. Abbreviations and symbols: **ELB**, endosteal lamellar bone; **IS**, intertrabecular space; **OPFB**, higher organization of parallel-fibered bone; **PAT**, pathology; **PFB**, parallel-fibered bone; **SF**, Sharpey's fibers; *, primary vascular canal; **red +**, primary osteon; **black and white +**, secondary osteon. Scale bars: 500 µm.

ZPAL V. 39/48 and ZPAL V. 39/49, the MiCL in *Proterochersis porebensis* is about 92% of the MaCL, which would make the MiCL of ZPAL V. 39/60 about 56 cm. This results in about the same MiCL as in *Proganochelys quenstedtii* SMF 09-F2 and is nearly as large as the largest individuals of the latter species. This indicates that the asymptotic adult size in both species could be similar, but it must be stressed that the growth curves were clearly different: ZPAL V. 39/48 is roughly the same size as SMNS 17203, but due to its high grade of ossification, ZPAL V. 39/48 can be regarded as representing an older individual. In ZPAL V. 39/48, the articular structures in the femur appear better ossified, the girdle and shell bones are fully fused, and there are no shell fontanelles (Szczygielski & Sulej 2016; Szczygielski *et al.* 2018); in contrast, SMNS 17203 has a rather simplified morphology of limb bones indicative of an extensive cartilaginous finish, open sutures between the girdle and shell bones, and large plastral fontanelles (Gaffney 1985, 1990). The ontogenetic stage of ZPAL V. 39/48 is better comparable with that of SMNS 16980, which is over 20% larger. Moreover, even the smallest complete shell of *Proterochersis porebensis*, ZPAL V. 39/34 (MiCL = MaCL = 28 cm), although morphologically juvenile and having unfused pelvic bones, has a fully ankylosed shell and no trace of fontanelles (Sulej *et al.* 2012; Szczygielski & Sulej 2016). These differences do not seem to be an effect of ecologically-driven shell ossification delay (fontanelle retention) in *Proganochelys quenstedtii*. On the contrary, that species is usually recovered as either terrestrial or less aquatic than *Proterochersis* spp., whereas shell histology and bromalite material from Poręba suggest that *Proterochersis porebensis* spent at least some of its lifetime in aquatic environment (Joyce & Gauthier 2004; Scheyer & Sander 2007; Benson *et al.* 2011; Lautenschlager *et al.* 2018; Bajdek *et al.* 2019; Dudgeon *et al.* 2021; Szczygielski & Słowiak 2022; Evers *et al.* 2022). Therefore, it seems likely that *Proganochelys quenstedtii* during early life stages grew faster than *Proterochersis porebensis* and attained distinctly larger body sizes at earlier ontogenetic stages. The linear correlation between the MiCL and humerus length calculated for *Palaeochersis talampayensis* (PULR 068) and *Proganochelys quenstedtii* (SMNS 16980, SMF 09-F2) is found to be significant ($r = 0.97$; $p < 0.01$) with a positive slope ($y = 1.2621 x - 0.99909$). The correlation calculated for the MiCL and femur length for *Proganochelys quenstedtii* (SMNS 16980, SMNS 17203, SMNS 17204) and *Proterochersis porebensis* (ZPAL V. 39/48) was also revealed to be significant ($r = 0.99$; $p < 0.001$) with a negative slope ($y = 0.89106 x - 0.31484$). The results imply that as the animal's size increases the proportional length of the femur decreases relative to MiCL in both *Proterochersis porebensis* and *Proganochelys quenstedtii* and the proportional length of the humerus increases relative to MiCL in *Proganochelys quenstedtii*. The linear correlation calculated for *Proganochelys quenstedtii* alone shows a similar tendency (non-significant positive correlation: $y = 1.063 x - 0.657$, $r = 0.97$, $p > 0.1$ for the humerus to MiCL; significant negative correlation: $y = 0.85 x - 0.24$, $r = 0.99$, $p < 0.01$ for the femur to MiCL), the results, however, are less significant due to the small sample size. See Appendices 5-16 for details.

It is also notable that there seems to be a proportional increase in bone robustness (particularly at the bases of the proximal and distal expansions) in the largest femur of *Proterochersis porebensis* (ZPAL V. 39/432) relative to other specimens (including the slightly smaller ZPAL V. 39/500), which is not observed in the available material of *Proganochelys quenstedtii* (note that although complete femora are only available for juvenile to young adult individuals, no particular increase in robusticity is also observed in fragments of larger adult femora; Jaekel 1916; Gaffney 1990). Although incomplete specimens are difficult to accurately evaluate in that respect, this is measurable for ZPAL V. 39/48 and ZPAL V. 39/432 (Table 4). That may imply that in *Proterochersis porebensis* the femora at more advanced ontogenetic stages grew in girth proportionally more than in length. This seems consistent with numerous vascular openings visible on the distal end of ZPAL V. 39/500, suggesting continued active growth, which seem to be absent in smaller specimens (e.g. ZPAL V. 39/26) and the slightly larger but more massive ZPAL V. 39/432. If the observed femur to MiCL ratio of 0.32 is used to calculate the studied *Proterochersis porebensis* individuals, ZPAL V. 39/432 is estimated to have the MiCL of 43.8 cm (MaCL about 47.5), i.e., slightly smaller than ZPAL V. 39/49. Values for other femora are provided in Table 5.

Another complication is that there are no specimens of *Proterochersis porebensis* consisting of associated shells and humeri. It is tempting to ascribe the humerus to midline carapace length ratio of about 0.27-0.28 and slight positive allometry of the humerus (shared between *Palaeochersis talampayensis* and *Proganochelys quenstedtii*) to *Proterochersis porebensis*, and roughly similar proportions are suggested by the size of the glenoid. While the exact length or height of the glenoid surface is in some cases difficult to measure due to damage, deformation, or the uncertainty concerning the cartilage covering, at least the coracoid facet of the glenoid in *Proganochelys quenstedtii* seems to be roughly the same width as the humeral head and shoulder (Table 6). The MiCL to humerus length ratio would imply that ZPAL V. 39/50 (10.6 cm long) would belong to an individual of MiCL about 37.9 cm (MaCL *c.* 41 cm), i.e., smaller than the subadult ZPAL V. 39/48. For ZPAL V. 39/156, 433, 439, and 446, the MiCL and MaCL values are given in Table 4. The maximum width of the coracoid glenoidal facet in ZPAL V. 39/48 is 2.6 cm, which agrees with the humeral head width of ZPAL V. 39/50 (2.7 cm). This, however, is somewhat problematic. Firstly, ZPAL V. 39/50 is an exceptionally well-ossified humerus with sharply defined morphological features (more so than in all known specimens of either *Proterochersis porebensis* and *Proganochelys quenstedtii*, except perhaps SMF 09-F2), indicating an advanced ontogenetic stage and lack of thick cartilaginous epiphysis. Secondly, obtained CT data reveal that its periosteal cortex is significantly affected by secondary remodeling and the boundary of the internal medullary region is unclear – an image reminiscent of adult, large bones such as SMF 09-F2 and ZPAL V. 39/500 rather than a subadult histomorphology. Thirdly, that would make the observed size distribution of recovered humeri of *Proterochersis porebensis* heavily skewed in favor of juveniles – out of 14 specimens,

TABLE 4. — *Proterochersis porebensis* Szczygielski & Sulej, 2016, massiveness of complete femora, calculations for digitized meshes.

Specimen	Length (mm)	Surface area (mm²)	Surface area/length	Volume (mm³)	Volume/length
ZPAL V. 39/48	127	10615.03	83.6	38710.24	304.8
ZPAL V. 39/432	140	14942.39	106.7	78496.05	560.7

TABLE 5. — Stylopodial bone lengths, midline carapace lengths (**MiCL**), and maximum carapace lengths (**MaCL**) for *Proterochersis porebensis* Szczygielski & Sulej, 2016. Incomplete humeri lengths estimated as 5.870655 distal depth (**DD**). Incomplete femora lengths estimated as 5.578671329 DD or extrapolated from proportions of complete femora (E). MiCL = humerus length / 0.28 or femur length / 0.32 (see text for discussion). MaCL = MiCL / 0.923889556 (based on average for complete carapaces ZPAL V. 39/48 and ZPAL V. 39/49). Estimated values indicated in **italics**. *****, In juvenile specimens MiCL = MaCL, as evidenced by ZPAL V. 39/34 (28 cm); therefore, the formula used here is not representative for them. Moreover, the available sample is too limited to determine whether they followed the same linear size correspondence as larger specimens or if a more accurate model should be proposed. Therefore, the estimates presented here must be treated as rough approximations.

Bone	Specimen	Length (cm)	MiCL (cm)	MaCL (cm)
Humerus	ZPAL V. 39/50	10.6	*37.9*	*41*
	ZPAL V. 39/157	*7.7*	*27.5*	*
	ZPAL V. 39/433	*8.2*	*29.3*	*31.9*
	ZPAL V. 39/439	*4.7*	*16.8*	*
Femur	ZPAL V. 39/432	14	*43.8*	*47.6*
		DD: *5.6*	DD: *17.5*	
	ZPAL V. 39/499	E: *8.8*	E: *27.5*	*
		DD: *12.8*	DD: *40*	DD: *43.5*
	ZPAL V. 39/500	E: *13*	E: *40.6*	E: *44.2*

TABLE 6. — Measurements of glenoid and humeral head in *Proganochelys quenstedtii* Baur, 1887 and *Proterochersis porebensis* Szczygielski & Sulej, 2016.

Species	Specimen number	Coracoid facet of glenoid maximal width [cm]	Humeral head width (including shoulder) [cm]
Proganochelys quenstedtii	SMNS 17203	L: 3.1	L: 3.1
	SMSN 16980	L: 3.5	L: 3.7
		R: 3.5	R: 3.4
Proterochersis porebensis	ZPAL V. 39/48	L: 2.6	–

ZPAL V. 39/50 is the second largest humerus (the poorly preserved and incomplete ZPAL V. 39/445 being slightly larger, but still likely smaller than, e.g. humeri of *Proganochelys quenstedtii* SMSN 16980). While such a preservation bias is not impossible, it is not observed for scapulocoracoids (at least 14 specimens, out of which seven are smaller than ZPAL V. 39/48), femora (13 specimens, eight smaller than ZPAL V. 39/48), or shell fragments (e.g. Szczygielski *et al.* 2018; Szczygielski & Słowiak 2022). Therefore, five scenarios (or their mix) should be considered:

– *Proterochersis porebensis*, *Proganochelys quenstedtii*, and *Palaeochersis talampayensis* all exhibit the same humerus to carapace length ratio and positive allometry, the size distribution of humeri from Poręba is skewed, ZPAL V. 39/50 belongs to an individual of a similar size as ZPAL V. 39/48, and its apparent advanced stage of ossification and remodeling is an effect of some ecological adaptation or pathology;

– *Proterochersis porebensis* has proportionally shorter humeri than *Proganochelys quenstedtii* and *Palaeochersis talampayensis* (analogically to the proportionally shorter femora in *Palaeochersis talampayensis* than in the former two species), the size distribution of humeri from Poręba is, therefore, not skewed, ZPAL V. 39/50 indeed represents an older, more ontogenetically advanced specimen, and correspondence between the glenoid and humerus size is obscured by missing articular cartilages;

– the shell-humerus size correspondence is similar between *Proterochersis porebensis*, *Proganochelys quenstedtii*, *Palaeochersis talampayensis*, and the size distribution of humeri from Poręba is indeed skewed, but ZPAL V. 39/50 represents an unusually small older individual; its advanced ossification stage is therefore explained by intraspecific size variability;

– the proportion of humeral and shell growth in *Proterochersis porebensis* followed a similar trajectory as in *Proganochelys quenstedtii* over some life period, but then the humeral growth slowed down allometrically, thus ZPAL V. 39/50 represents a more advanced ontogenetic stage than ZPAL V. 39/48 but its similar size is an expected consequence of changed growth trajectory; still, large humeri are in that case underrepresented in Poręba;

– the shell to humeral length ratio could be the same or different in *Proterochersis porebensis* and other Triassic taxa but there is some unrecognized sexual size dimorphism in the population of *Proterochersis porebensis* and therefore ZPAL V. 39/48 may be a subadult individual of the larger

sex while ZPAL V. 39/50 belongs to an older individual of the smaller sex; the observed size distribution is, nonetheless, skewed in favor of smaller, less ossified specimens.

Given the lack of meaningful anatomical differences and lack of evidence of other turtle taxa in Poręba, e.g. based on shell finds (Szczygielski & Sulej 2016, 2019; Szczygielski *et al.* 2018; Szczygielski & Słowiak 2022), taxonomic separation between ZPAL V. 39/48 and ZPAL V. 39/50 is here considered unlikely. This issue can only be solved by future finds of associated proterochersid humeri and shells. In any case, the examined stylopodial bones of *Proterochersis porebensis* clearly represent a wide spectrum of sizes and ontogenetic stages, at least the large femora (ZPAL V. 39/432, ZPAL V. 39/500) likely belong to adult individuals but not yet approaching the asymptotic body size. Therefore, they are likely ontogenetically younger than *Proganochelys quenstedtii* SMF 09-F2. Moreover, although *Proterochersis porebensis* and *Proganochelys quenstedtii* could reach similar maximal body sizes, their growth trajectories were clearly different.

Comparison of long bone histology of *Proterochersis porebensis* and *Proganochelys quenstedtii*

Both taxa show a very similar microanatomy and share histological characters. The primary tissue and vascularization consist of moderate to poorly vascularized parallel-fibered matrix in both taxa. Simple vascular canals are mainly longitudinally oriented, and a few primary osteons are developed along all samples. The humeral sample of *Proganochelys quenstedtii* shows a higher grade of remodeling compared to the middle-sized humerus of *Proterochersis porebensis* (ZPAL V. 39/433), which likely is the result of an older ontogenetic stage.

DISCUSSION

The stem turtles *Proterochersis porebensis* and *Proganochelys quenstedtii* do not differ significantly from other non-marine turtles in terms of their limb histology (primarily consisting of parallel-fibered bone in a poorly to moderately vascularized cortex, medullary region filled with trabeculae retaining remnants of primary tissue, etc. – compare with references in the Introduction). They both exhibit the typical derived non-marine turtle histology and microanatomy, which is relatively distinct (mainly in terms of microanatomy; i.e., the absence of a medullary cavity and the presence of a well-developed and expanding cancellous medullary region during ontogeny) from the histologically studied non-testudinate pantestudinates (Lyson *et al.* 2016; Schoch *et al.* 2019). The humeri and femora studied herein share a thick and compact, weakly vascularized cortex with the juvenile humerus of *Eunotosaurus africanus* Seeley, 1892 presented by Lyson *et al.* 2016) and the humerus and femur of *Pappochelys rosinae* Schoch & Sues, 2015 presented by Schoch *et al.* (2019), however, they generally differ from both in the lack of a central medullary cavity. In that regard, the only exception is the large femur ZPAL V. 39/432, which does show a small (albeit proportionally of similar size to that seen in *Pappochelys rosinae*; Schoch *et al.* 2019) cavity surrounded by a thick network of trabeculae. The CT cross sections of a humerus and femur of *Proganochelys quenstedtii* published by Nakajima (2017) and Schoch *et al.* (2019: supplementary material) appear to have a thicker cortex than the small humerus and femur of *Proterochersis porebensis*, ZPAL V. 39/439 and ZPAL V. 39/499, but more restricted cancellous region compared to the large femora ZPAL V. 39/432 and ZPAL V. 39/500, and more homogenous density in that region compared to the large humerus ZPAL V. 39/50. In those respects, they are the most similar structurally to the middle-sized humerus, ZPAL V. 39/439. That seems appropriate given their respective size and developmental stage, as the *Proganochelys quenstedtii* individual in question is interpreted as a subadult (Gaffney 1990), but that structural difference may also represent a taxonomic character. Significant changes to turtle long bone histology between the forelimb and hindlimb and during ontogeny were noted, e.g. by Botha (2017), Botha & Botha (2019), and Bhat *et al.* (2019). Mainly the latter makes comparisons with older literature data, which unfortunately often lack information on the ontogenetic age of sampled specimens, difficult, especially because in many cases only close-ups rather than whole cross-sections are presented.

In general, the microstructure and histology in *Proterochersis porebensis* and *Proganochelys quenstedtii* is similar to that observed in *Stigmochelys pardalis* and *Testudo* spp. (Castanet & Cheylan 1979; Botha 2017; Botha & Botha 2019), and the changes occurring in age are overall consistent between these taxa, supporting the interpretation that ZPAL V. 39/439 and ZPAL V. 39/499 represent juveniles (older than the ones sectioned by Botha 2017 and Botha & Botha 2019 but younger than their early subadults), ZPAL V. 39/433 a subadult, and ZPAL V. 39/500 an adult (distinctly more remodelled than the late subadults of Botha 2017 and Botha & Botha 2019). This assumption is also consistent with the classes used for *Proterochersis porebensis* in previous works based on the body size and stage of shell development (Szczygielski & Sulej 2016; Szczygielski *et al.* 2018; Szczygielski & Słowiak 2022). Likewise, the general histological structure of the humerus resembles that of *Chelonoidis chilensis* and *Phrynops hilarii* presented by Pereyra *et al.* (2019) and Pereyra (2022), but is less compact (possibly partly due to the differences in the sectioning planes). The similarities to *Chersina angulata* are less pronounced, particularly in post-juvenile specimens (Bhat *et al.* 2019), due to the more random vascularization, asymmetric growth, and significant presence of woven and fibrolamellar bone in that taxon, despite *Chersina angulata*, *Chelonoidis chilensis*, *Stigmochelys pardalis*, and *Testudo* spp. all representing the same clade (Cryptodira: Testudinidae), possibly partly due to the size and bone geometry difference between the taxa. In contrast to the testudinid species, our samples of *Proterochersis porebensis* do not show a sub-plexiform arrangement of vasculature (Botha 2017; Bhat *et al.* 2019; Botha & Botha 2019). The histology of femora of younger specimens of the podocnemidid (Pleurodira) *Podocnemis expansa* (Schweigger 1812) also differs in the presence of a more randomly organized vascularization, but becomes more

similar with maturity (Chinsamy & Valenzuela 2008). The chelyid (Pleurodira) *Hydromedusa tectifera* and *Yaminuchelys maior* present a comparable histology to *Proterochersis porebensis*. However, the bones are compact in *H. tectifera*. Moreover, specimens designated by Pereyra *et al.* (2020) and Pereyra (2022) as adults compare better to the subadult observed in our samples and in the testudinids (Castanet & Cheylan 1979; Botha 2017; Botha & Botha 2019; Bhat *et al.* 2019).

The large femur ZPAL V. 39/500 shows a significant resorption of the cortex and relatively thin trabeculae, giving a somewhat osteoporotic appearance. This may be simply because of the mature age of the individual. Nakajima *et al.* (2014) noted increased bone resorption in humeri of large terrestrial turtles and appearance of small cavities in the cortical areas of particularly large species and Botha & Botha (2019) and Castanet & Cheylan (1979) also observed a decrease of compactness in humeri and femora of adult *Stigmochelys pardalis* and *Testudo* spp. compared to subadults, and presented a very similar pattern of secondary remodeling as we observed in ZPAL V. 39/500. Unfortunately, mature stages of ontogeny in these studies were represented only by singular individuals and no information was provided about their sex. Suzuki (1963) discovered that femora in modern turtles may serve as a calcium reservoir for egg-bearing, mature females, producing a similar osteoporotic microstructure, but detected no such changes in male and immature individuals. Although speculative, it seems, therefore, possible that ZPAL V. 39/500 could have belonged to a mature female. An osteoporosis-like change of a hypothetically similar origin (although not observed in modern turtles; Suzuki 1963) was also noticed in the carapace of a large individual of *Proterochersis porebensis* (ZPAL V. 39/61) by Szczygielski & Słowiak (2022). Interestingly, the cortex of ZPAL V. 39/432 appears to be less vascularized (and, supposedly, less remodeled) than in ZPAL V. 39/500, even accounting for the more distal section plane of the latter relative to the ossification center, despite ZPAL V. 39/432 being slightly larger and clearly more robust. This apparent difference in secondary vascularization may partly be explained by the limited resolution of the CT scan possibly obscuring thinner vascular structures. However, the resolution is sufficient to observe fine vascular canals in other specimens and intertrabecular cavities in that specimen (the size of which in ZPAL V. 39/500 is of the same order of magnitude as that of the secondary osteons invading the cortex). Moreover, it is the tissue in ZPAL V. 39/500 which is divergent relative to other specimens. Therefore, intraspecific (ontogenetic or sexual) and/or seasonal (related to egg production and oviposition, as explained above) variability may be a better explanation.

Unlike in most tetrapods, vascular density is usually lower in terrestrial and semiaquatic turtles than in fully aquatic species; however, due to significant variability within and overlap between ecotypes, it is frequently difficult to distinguish between terrestrial and semiaquatic turtles based on long bone microstructure alone (e.g. Ricqlès *et al.* 2004; Germain & Laurin 2005; Kriloff *et al.* 2008; Canoville & Laurin 2010; Laurin *et al.* 2011; Nakajima *et al.* 2014; Botha 2017; Botha & Botha 2019; Sena *et al.* 2021; Pereyra 2022). Lifestyle assessments performed by Germain & Laurin (2005) based on radii microstructure tended to overestimate the aquatic adaptations in most of the examined turtle species, i.e., terrestrial turtles were recovered as amphibious, one amphibious as aquatic, and only in one case an amphibious species was recovered as terrestrial; estimations proved correct only for fully aquatic taxa. Similar error, with most terrestrial and some aquatic turtle taxa wrongly assessed, was detected in the case of estimates based on tibiae (Kriloff *et al.* 2008) and humeri (Canoville & Laurin 2010). Botha (2017) and Botha & Botha (2019) calculated compactness indices for humeri, radii, ulnae, femora, tibiae, and fibulae of varied ontogenetic ages of the terrestrial *Stigmochelys pardalis* and obtained variable values between the bones and individuals, but predominantly suggesting a fully aquatic lifestyle. This variability is also true for the specimens sectioned here. Depending on the bone (humerus vs femur) and size (ontogenetic age), the vascular density, thickness of the cortex, extent of the cancellous area, and relative size of trabeculae and intertrabecular spaces are vastly different. Nonetheless, the cortices, especially in post-juvenile bones are surprisingly thick, even in the thin sections despite the fact that they were taken well below the most compact area. Unsurprisingly, however, the microstructure at the level of the growth center overall fits within the spectrum documented by Canoville & Laurin (2010) and Nakajima *et al.* (2014) for extant terrestrial and semiaquatic turtles.

CONCLUSION

Overall, the comparison of limb bone histology of both examined species reveals that general microstructural patterns typical for Recent turtle appendicular bones were established already in the Triassic, but at the same time the earliest turtle representatives already diverged, e.g. in growth strategies. Future finds and data may allow a more precise understanding on the degree of variability between those taxa and, possibly, its correlation with the environment, locomotory adaptations, or phylogeny.

Acknowledgements
We thank Tomasz Sulej (Institute of Paleobiology, Polish Academy of Sciences) and all the participants of te excavations in Poręba for their collecting efforts and partial preparation of the material of *Proterochersis porebensis*. Moreover, we thank Piotr Duda (Faculty of Exact and Technical Sciences, University of Silesia in Katowice) for CT scanning of the specimens, Adam Zaremba (Institute of Paleobiology, Polish Academy of Sciences, Warsaw) for preparation of thin sections, and Michał Surowski (Faculty of Geology, University of Warsaw) for photography of thin sections. We thank the Saurierkomission Frick and Andrea Oettl (SMF) for access to the *Proganochelys* specimen exhibited in Frick. We also thank the two reviewers for their comments on the manuscript.

Funding
The study of *Proterochersis porebensis* limb histology was funded by the National Science Centre, Poland (grant 2020/39/B/NZ8/01074 to T. Szczygielski) and TMS acknowledges support by the Swiss National Science Foundation (grant no. 31003A_179401).

Data availability
CT scan data and 3D models of the studied *Proganochelys quenstedtii* and *Proterochersis porebensis* humeri and femora are made available on Morphosource repository project ID: https://www.morphosource.org/projects/000532724.

REFERENCES

Amprino R. & Godina G. 1947. — La struttura della ossa nei vertebrati. Ricerche comparative negli anfibi e negli amnioti. *Pontificia Academia Scientarum, Commentationes* 11 (9): 229-464.

Avens L. & Goshe L. R. 2007. — Comparative skeletochronological analysis of Kemp's ridley (*Lepidochelys kempii*) and loggerhead (*Caretta caretta*) humeri and scleral ossicles. *Marine Biology* 152 (6): 1309-1317. https://doi.org/10.1007/s00227-007-0779-9

Avens L. & Snover M. L. 2013. — Age and age estimation in sea Turtles, *in* Wyneken J., Lohmann K. J. & Musick J. A. (eds.), *The Biology of Sea Turtles*. Vol. III. CRC Press, Boca Raton, London, New York: 97-133. https://doi.org/10.1201/b13895-6

Avens L., Taylor J. C., Goshe L. R., Jones T. T. & Hastings M. 2009. — Use of skeletochronological analysis to estimate the age of leatherback sea turtles *Dermochelys coriacea* in the western North Atlantic. *Endangered Species Research* 8 (3): 165-177. https://doi.org/10.3354/esr00202

Avens L., Goshe L. R., Harms C. A., Anderson E. T., Hall A. G., Cluse W. M., Godfrey M. H., McNeill J. B., Stacy B., Bailey R. & Lamont M. M. 2012. — Population characteristics, age structure, and growth dynamics of neritic juvenile green turtles in the northeastern Gulf of Mexico. *Marine Ecology Progress Series* 458: 213-229. https://doi.org/10.3354/meps09720

Avens L., Goshe L. R., Pajuelo M., Bjorndal K. A., MacDonald B. D., Lemons G. E., Bolten A. B. & Seminoff J. A. 2013. — Complementary skeletochronology and stable isotope analyses offer new insight into juvenile loggerhead sea turtle oceanic stage duration and growth dynamics. *Marine Ecology Progress Series* 491: 235-251. https://doi.org/10.3354/meps10454

Avens L., Goshe L. R., Coggins L., Snover M. L., Pajuelo M., Bjorndal K. A. & Bolten A. B. 2015. — Age and size at maturation- and adult-stage duration for loggerhead sea turtles in the western North Atlantic. *Marine Biology* 162 (9): 1749-1767. https://doi.org/10.1007/s00227-015-2705-x

Bailleul A., Ségalen L., Buscalioni A. D., Cambra-Moo O. & Cubo J. 2011. — Palaeohistology and preservation of tetrapods from Las Hoyas (Lower Cretaceous, Spain). *Comptes Rendus Palevol* 10 (5-6): 367-380. https://doi.org/10.1016/j.crpv.2011.05.002

Bajdek P., Szczygielski T., Kapuścińska A. & Sulej T. 2019. — Bromalites from a turtle-dominated fossil assemblage from the Triassic of Poland. *Palaeogeography, Palaeoclimatology, Palaeoecology* 520: 214-228. https://doi.org/10.1016/j.palaeo.2019.02.002

Ballerstedt M. 1922. — Über das plastron der schildkröten des keupers und die gestalt der panzerschale von *Proganochelys quenstedtii* Baur nach dem Tübinger fossil. *Palaeontologische Zeitschrift* 4 (1): 64-74. https://doi.org/10.1007/BF03041559

Balli A. 1937. — Observazioni sulla architettura delle oassa lunghe nei rettili. *Archivo Zoologico Italiano* 24: 419-441.

Baur G. 1887. — Ueber den ursprung der extremitäten der Ichthyopterygia. *Berichte über de Versammlungen des Oberrheinischen Vereines* 20: 17-20.

Baur G. 1893. — Notes on the classification of the Cryptodira. *American Naturalist* 27 (319): 672-675.

Bell T. 1828. — Descriptions of three new species of land tortoises. *Zoological Journal* 3: 419-421.

Benson R. B. J., Domokos G., Várkonyi P. L. & Reisz R. R. 2011. — Shell geometry and habitat determination in extinct and extant turtles (Reptilia: Testudinata). *Paleobiology* 37 (4): 547-562. https://doi.org/10.1666/10052.1

Bhat M. S., Chinsamy A. & Parkington J. 2019. — Long bone histology of *Chersina angulata*: interelement variation and life history data. *Journal of Morphology* 280 (12): 1881-1899. https://doi.org/10.1002/jmor.21073

Bhat M. S., Chinsamy A. & Parkington J. 2023. — Bone histology of Neogene angulate tortoises (Testudines: Testudinidae) from South Africa: palaeobiological and skeletochronological implications. *Royal Society Open Science* 10 (3): 230064. https://doi.org/10.1098/rsos.230064

Bjorndal K. A., Bolten A. B., Bennett R. A., Jacobson E. R., Wronski T. J., Valeski J. J. & Eijazar P. J. 1998. — Age and growth in sea turtles: limitations of skeletochronology for demographic studies. *Copeia* 1998 (1): 23-30. https://doi.org/10.2307/1447698

Botha A. E. 2017. — *Comparative bone histology of* Stigmochelys pardalis *(leopard tortoise), with specific reference to ontogeny and biomechanics*. M.Sc. thesis, University of the Free State, 81 p. http://hdl.handle.net/11660/6462

Botha A. E. & Botha J. 2019. — Ontogenetic and interelemental osteohistological variability in the leopard tortoise Stigmochelys pardalis. *PeerJ* (7): e8030. https://doi.org/10.7717/peerj.8030

Braun L. 1920. — Geologische Beschreibung von Blatt Frick (1 : 25 000) im Aargauer Tafeljura. *Verhandlungen der Naturforschenden Gesellschaft zu Basel* 31: 189-242.

Cadena E. A., Scheyer T. M., Carrillo-Briceño J. D., Sánchez R., Aguilera-Socorro O. A., Venegas A., Pardo M., Hansen D. M. & Sánchez-Villagra M. R. 2020. — The anatomy, paleobiology, and evolutionary relationships of the largest extinct side-necked turtle. *Science Advances* 6 (7): eaay4593. https://doi.org/10.1126/sciadv.aay4593

Canoville A. & Laurin M. 2010. — Evolution of humeral microanatomy and lifestyle in amniotes, and some comments on palaeobiological inferences. *Biological Journal of the Linnean Society* 100 (2): 384-406. https://doi.org/10.1111/j.1095-8312.2010.01431.x

Casale P., Conte N., Freggi D., Cioni C. & Argano R. 2011. — Age and growth determination by skeletochronology in loggerhead sea turtles (*Caretta caretta*) from the Mediterranean Sea. *Scientia Marina* 75 (1): 197-203. https://doi.org/10.3989/scimar.2011.75n1197

Castanet J. 1985. — La squelettochronologie chez les Reptiles. I. Résultats expérimentaux sur la signification des marques de croissance squelettiques ches les lézards et les tortues. *Annales des Sciences Naturelles, Zoologie* 7: 23-40.

Castanet J. 1987. — La squelettochronologie chez les Reptiles. III. Application. *Annales des Sciences Naturelles, Zoologie* 8: 157-172.

Castanet J. 1988. — Les méthodes d'estimation de l'age chez les chéloniens. *Mésogée* 48: 21-28.

Castanet J. 1994. — Age estimation and longevity in reptiles. *Gerontology* 40 (2-4): 174-192. https://doi.org/10.1159/000213586

Castanet J. & Cheylan M. 1979. — Les marques de croissance des os et des écailles comme indicateur de l'âge chez *Testudo hermanni* et *Testudo graeca* (Reptilia, Chelonia, Testudinidae). *Canadian Journal of Zoology* 57 (8): 1649-1665. https://doi.org/10.1139/z79-216

CERDA I. A., PEREYRA M. E., GARRONE M., PONCE D., NAVARRO T. G., GONZÁLEZ R., MILITELLO M., LUNA C. A. & JANNELLO J. M. 2020. — A basic guide for sampling and preparation of extant and fossil bones for histological studies. *Publicación Electrónica de la Asociación Paleontológica Argentina* 20 (1): 15-28. https://doi.org/10.5710/PEAPA.07.04.2020.314

CHALOUPKA M. & MUSICK J. A. 1997. — Age, growth and population dynamics, *in* LUTZ P. L. & MUSICK J. A. (eds), *The Biology of Sea Turtles*. CRC Press, New York: 233-276.

CHEYLAN M. 1981. — Biologie et écologie de la tortue d'Hermann *Testudo hermanni*, Gmelin 1789. Contribution de l'espèce à la connaissance des climats quaternaires de la France. *Mémoires et Travaux de l'Institut de Montpellier* 13: 1-383.

CHINSAMY A. & VALENZUELA N. 2008. — Skeletochronology of the endangered side-neck turtle, *Podocnemis expansa*. *South African Journal of Science* 104 (7-8): 311-314.

ÇIÇEK K., KUMAŞ M., AYAZ D. & TOK C. V. 2016. — A skeletochronological study of age, growth and longevity in two freshwater turtles, *Emys orbicularis* and *Mauremys rivulata*, from Mediterranean Turkey (Reptilia: Testudines). *Zoology in the Middle East* 62 (1): 29-38. https://doi.org/10.1080/09397140.2016.1144277

CIGNONI P., CALLIERI M., CORSINI M., DELLEPIANE M., GANOVELLI F. & RANZUGLIA G. 2008. — MeshLab: an open-source mesh processing tool: 129-136. https://doi.org/10.2312/LocalChapterEvents/ItalChap/ItalianChapConf2008/129-136

COLES W. C., MUSICK J. A. & WILLIAMSON L. A. 2001. — Skeletochronology validation from an adult loggerhead (*Caretta caretta*). *Copeia* 2001 (1): 240-242. https://doi.org/fm4zdh

COPE E. D. 1869. — Seventh contribution to the herpetology of tropical America. *Proceedings of the American Philosophical Society* 11: 147-192.

COPE E. D. 1871. — [Preliminary report of expedition into the Valley of the Smoky Hill river, Kansas, and descriptions of new fossil sauroids and chelonians discovered and collected there]. *Proceedings of the American Philosophical Society* 12 (86): 174-176.

COPE E. D. 1873. — [Additional specimen of the turtle from the Cretaceous of Kansas]. *Proceedings of the Academy of Natural Sciences of Philadelphia* 25 (1): 10.

CRAWFORD G. N. C. 1940. — The evolution of the Haversian pattern in bone. *Journal of Anatomy* 74 (2): 284-299.

CUBO J., LEGENDRE P., RICQLÈS A. J. DE, MONTES L., DE MARGERIE E., CASTANET J. & DESDEVISES Y. 2008. — Phylogenetic, functional, and structural components of variation in bone growth rate of amniotes. *Evolution and Development* 10 (2): 217-227. https://doi.org/10.1111/j.1525-142X.2008.00229.x

CUBO J., LE ROY N., MARTINEZ-MAZA C. & MONTES L. 2012. — Paleohistological estimation of bone growth rate in extinct archosaurs. *Paleobiology* 38 (2): 335-349. https://doi.org/10.1666/08093.1

CURTIN A. J., ZUG G. R., MEDICA P. A. & SPOTILA J. R. 2008. — Assessing age in the desert tortoise *Gopherus agassizii*: testing skeletochronology with individuals of known age. *Endangered Species Research* 5 (1): 21-27. https://doi.org/10.3354/esr00108

CZEPIŃSKI Ł., DRÓŻDŻ D., SZCZYGIELSKI T., TAŁANDA M., PAWLAK W., LEWCZUK A., RYTEL A. & SULEJ T. 2021. — An Upper Triassic terrestrial vertebrate assemblage from the forgotten Kocury locality in southern Poland with a new aetosaur taxon. *Journal of Vertebrate Paleontology* 41 (1): e1898977. https://doi.org/10.1080/02724634.2021.1898977

DANILOV I. G., OBRAZTSOVA E. M., BOITSOVA E. A. & SKUTSCHAS P. P. 2018. — Diversity of Middle Jurassic turtles from the Berezovsk Quarry locality, Krasnoyarsk Region, Russia: morphology and histological study. *Paleontological Journal* 52 (2): 188-200. https://doi.org/10.1134/S0031030118010070

DUDGEON T. W., LIVIUS M. C. H., ALFONSO N., TESSIER S. & MALLON J. C. 2021. — A new model of forelimb ecomorphology for predicting the ancient habitats of fossil turtles. *Ecology and Evolution* 11 (23): 17071-17079. https://doi.org/10.1002/ece3.8345

DUMÉRIL A. M. C. & BIBRON G. 1835. — *Erpétologie générale ou Histoire naturelle complète des reptiles*. Tome Second. Roret, Paris, 680 p.

DZIOMBER L., JOYCE W. G. & FOTH C. 2020. — The ecomorphology of the shell of extant turtles and its applications for fossil turtles. *PeerJ* 8: e10490. https://doi.org/10.7717/peerj.10490

EHRET D. J. 2007. — Skeletochronology: a method for determing the individual age and growth of modern and fossil tortoises (Reptilia: Testudines). *Florida Museum of Natural History Bulletin* 47 (2): 49-72.

ENLOW D. H. 1969. — The bone of reptiles, *in* GANS C. (ed.), *Biology of the Reptilia. Volume 1. Morphology A*. Academic Press, London; New York: 46-81.

ENLOW D. H. & BROWN S. O. 1957. — A comparative histological study of fossil and recent bone tissues. Part II. *Texas Journal of Science* 9 (2): 186-214.

EVERS S. W., JOYCE W. G., CHOINIERE J. N., FERREIRA G. S., FOTH C., HERMANSON G., YI H., JOHNSON C. M., I. & BENSON R. B. J. 2022. — Independent origin of large labyrinth size in turtles. *Nature Communications* 13 (1): 5807. https://doi.org/10.1038/s41467-022-33091-5

FEDOROV A., BEICHEL R., KALPATHY-CRAMER J., FINET J., FILLION-ROBIN J.-C., PUJOL S., BAUER C., JENNINGS D., FENNESSY F. M., SONKA M., BUATTI J., AYLWARD S. R., MILLER J. V., PIEPER S. & KIKINIS R. 2012. — 3D Slicer as an image computing platform for the quantitative imaging network. *Magnetic Resonance Imaging* 30 (9): 1323-1324. https://doi.org/10.1016/j.mri.2012.05.001

FOOTE J. S. 1911. — The comparative histology of femoral bones. *Transactions of American Microscopical Society* 30 (2): 87-140. https://doi.org/10.2307/3221427

FOOTE J. S. 1916. — A contribution to the comparative histology of the femur. *Smithsonian Contributions to Knowledge* 35 (3): 242.

FRAAS E. 1899. — *Proganochelys quenstedtii* Baur (*Psammochelys keuperina* Qu.). Einer neuer Fund der Keuperschildkröte aus dem Stubensandstein. *Jahreshefte des Vereins für Vaterländische Naturkunde in Württemberg* 55: 401-423.

FRAAS E. 1913. — *Proterochersis*, eine pleurodire Schildkröte aus dem Keuper. *Jahreshefte des Vereins für Vaterländische Naturkunde in Württemberg* 69: 13-30.

GAFFNEY E. S. 1985. — The shell morphology of the Triassic turtle *Proganochelys*. *Neues Jahrbuch für Geologie und Paläontologie - Abhandlungen* 170 (1): 1-26. https://doi.org/10.1127/njgpa/170/1985/1

GAFFNEY E. S. 1990. — The comparative osteology of the Triassic turtle *Proganochelys*. *Bulletin of the American Museum of Natural History* 194: 1-263.

GERMAIN D. & LAURIN M. 2005. — Microanatomy of the radius and lifestyle in amniotes (Vertebrata, Tetrapoda). *Zoologica Scripta* 34 (4): 335-350. https://doi.org/10.1111/j.1463-6409.2005.00198.x

GÔNET J., BARDIN J., GIRONDOT M., HUTCHINSON J. R. & LAURIN M. 2023. — Deciphering locomotion in reptiles: application of elliptic Fourier transforms to femoral microanatomy. *Zoological Journal of the Linnean Society* 198 (4): 1070-1091. https://doi.org/10.1093/zoolinnean/zlad006

GOSHE L. R., AVENS L., BYBEE J. & HOHN A. A. 2009. — An evaluation of histological techniques used in skeletochronological age estimation of sea turtles. *Chelonian Conservation and Biology* 8 (2): 217-222. https://doi.org/10.2744/CCB-0777.1

GOSHE L. R., AVENS L., SCHARF F. S. & SOUTHWOOD A. L. 2010. — Estimation of age at maturation and growth of Atlantic green turtles (*Chelonia mydas*) using skeletochronology. *Marine Biology* 157 (8): 1725-1740. https://doi.org/10.1007/s00227-010-1446-0

GRAY J. E. 1870. — Notce of a new Chilian tortoise (*Testudo chilensis*). *The Annals and Magazine of Natural History, Including Zoology, Botany, and Geology* 6: 190.

GROSS W. 1934. — Die Typen des mikroskopischen Knochenbaues bei fossilen Stegocephalen und Reptilien. *Zeitschrift für Anatomie und Entwicklungsgeschichte* 103 (6): 731-764. https://doi.org/10.1007/BF02118752

Haines R. W. 1938. — The primitive form of epiphysis in the long bones of tetrapods. *Journal of Anatomy* 72 (3): 323-343.
Haines R. W. 1942. — The evolution of epiphyses and of endochondral bone. *Biological Reviews* 17 (4): 267-292. https://doi.org/10.1111/j.1469-185X.1942.tb00440.x
Haines R. W. 1969. — Epiphyses and Sesamoids, *in* Gans C. (ed.), *Biology of the Reptilia. Volume 1. Morphology A*. Academic Press, London; New York: 81-115.
Hammer D. A. 1969. — Parameters of a marsh snapping turtle population. *Journal of Wildlife Diseases* 33 (4): 995-1005. https://doi.org/10.2307/3799337
Hammer Ø., Harper D. A. T. & Ryan P. D. 2001. — PAST: PAleontological STatistics software package for education and data analysis. *Palaeontologia Electronica* 4 (1): 1-9.
Horner J. R., Padian K. & Ricqlès A. J. de 2001. — Comparative osteohistology of some embryonic and perinatal archosaurs: developmental and behavioral implications for dinosaurs. *Paleobiology* 27 (1): 39-58. https://doi.org/drb943
Houssaye A. 2013. — Bone histology of aquatic reptiles: what does it tell us about secondary adaptation to an aquatic life? *Biological Journal of the Linnean Society* 108: 3-21. https://doi.org/10.1111/j.1095-8312.2012.02002.x
Jaekel O. 1914. — Über die Wirbeltierfunde aus der oberen Trias von Halberstadt. *Paläontologische Zeitschrift* 1 (1): 155-215. https://doi.org/10.1007/BF03160336
Jaekel O. 1916. — Die Wirbeltierfunde aus dem Keuper von Halberstadt. Serie II. Testudinata. *Palaeontologische Zeitschrift* 2 (3): 88-214. https://doi.org/10.1007/BF03160328
Jordan P., Pietsch J. S., Bläsi H., Furrer H., Kündig N., Looser N., Wetzel A. & Deplazes G. 2016. — The middle to late Triassic Bänkerjoch and Klettgau formations of northern Switzerland. *Swiss Journal of Geosciences* 109 (2): 257-284. https://doi.org/10.1007/s00015-016-0218-3
Joyce W. G. 2017. — A review of the fossil record of basal Mesozoic turtles. *Bulletin of the Peabody Museum of Natural History* 58 (1): 65-113. https://doi.org/10.3374/014.058.0105
Joyce W. G. & Gauthier J. A. 2004. — Palaeoecology of Triassic stem turtles sheds new light on turtle origins. *Proceedings of the Royal Society of London B: Biological Sciences* 271 (1534): 1-5.
Kikinis R., Pieper S. D. & Vosburgh K. 2014. — 3D Slicer: a platform for subject-specific image analysis, visualization, and clinical support, *in* Jolesz F. A. (ed.), *Intraoperative imaging image-guided therapy*. Springer, New York: 277-289. https://doi.org/10.1007/978-1-4614-7657-3_19
Klinger R. C. & Musick J. A. 1992. — Annular growth layers in juvenile loggerhead turtles (*Caretta caretta*). *Bulletin of Marine Science* 51 (2): 224-230.
Klinger R. C. & Musick J. A. 1995. — Age and growth of loggerhead turtles (*Caretta caretta*) from Chesapeake Bay. *Copeia* 1995 (1): 204-209. https://doi.org/10.2307/1446816
Kriloff A., Germain D., Canoville A., Vincent P., Sache M. & Laurin M. 2008. — Evolution of bone microanatomy of the tetrapod tibia and its use in palaeobiological inference. *Journal of Evolutionary Biology* 21 (3): 807-826. https://doi.org/10.1111/j.1420-9101.2008.01512.x
Kubik R., Uhl D. & Marynowski L. 2015. — Evidence of wildfires during deposition of the Upper Silesian Keuper succession, southern Poland. *Annales Societatis Geologorum Poloniae* 85: 685-696.
Laurin M., Canoville A. & Germain D. 2011. — Bone microanatomy and lifestyle: a descriptive approach. *Comptes Rendus Palevol* 10 (5-6): 381-402. https://doi.org/10.1016/j.crpv.2011.02.003
Lautenschlager S., Ferreira G. de S. & Werneburg I. 2018. — Sensory evolution and ecology of early turtles revealed by digital endocranial reconstructions. *Frontiers in Ecology and Evolution* 6: 7. https://doi.org/10.3389/fevo.2018.00007
Leidy J. 1851. — April 15th. *Proceedings of the Academy of Natural Sciences of Philadelphia* 5: 172-173.
Lenz A. J., Avens L., Campos Trigo C. & Borges-Martins M. 2016. — Skeletochronological estimation of age and growth of loggerhead sea turtles (*Caretta caretta*) in the western South Atlantic Ocean. *Austral Ecology* 41 (5): 580-590. https://doi.org/10.1111/aec.12347
Li C., Wu X., Rieppel O., Wang L. & Zhao L. 2008. — An ancestral turtle from the Late Triassic of southwestern China. *Nature* 456 (7221): 497-501. https://doi.org/10.1038/nature07533
Lichtig A. J. & Lucas S. G. 2017. — A simple method for inferring habitats of extinct turtles. *Palaeoworld* 26 (3): 581-588. https://doi.org/10.1016/j.palwor.2017.02.001
Linnaeus C. 1758. — *Systema naturae per regna tria naturae, secundum classes, ordines, genera, species, cum characteribus, differentiis, synonymis, locis. T. I*. Holmiae, Laurentii Salvii, Stockholm, 844 p.
Lyson T. R., Rubidge B. S., Scheyer T. M., De Queiroz K., Schachner E. R., Smith R. M. H., Botha-Brink J. & Bever G. S. 2016. — Fossorial origin of the turtle shell. *Current Biology* 26 (14): 1887-1894. https://doi.org/10.1016/j.cub.2016.05.020
MacCulloch R. D. & Secoy D. M. 1983. — Demography, growth, and food of western painted turtles *Chrysemys picta bellii* (Gray), from southern Saskatchewan. *Canadian Journal of Zoology* 61 (7): 1499-1509. https://doi.org/10.1139/z83-202
Mattox N. T. 1936. — Annular rings in the long bones of turtles and their correlation with size. *Transactions of the Illinois State Academy of Science* 28: 255-256.
Montes L., Le Roy N., Perret M., Buffrénil V. de, Castanet J. & Cubo J. 2007. — Relationships between bone growth rate, body mass and resting metabolic rate in growing amniotes: a phylogenetic approach. *Biological Journal of the Linnean Society* 92 (1): 63-76. https://doi.org/10.1111/j.1095-8312.2007.00881.x
Montes L., Castanet J. & Cubo J. 2010. — Relationship between bone growth rate and bone tissue organization in amniotes: first test of Amprino's rule in a phylogenetic context. *Animal Biology* 60 (1): 25-41. https://doi.org/10.1163/157075610x12610595764093
Motani R. & Vermeij G. J. 2021. — Ecophysiological steps of marine adaptation in extant and extinct non-avian tetrapods. *Biological Reviews* 96 (5): 1769-1798. https://doi.org/10.1111/brv.12724
Nakajima Y. 2017. — Turtle bone histology illuminate a new perspective on paleoecological reconstruction. *Journal of Fossil Research* 50 (1): 22-27
Nakajima Y., Hirayama R. & Endo H. 2014. — Turtle humeral microanatomy and its relationship to lifestyle. *Biological Journal of the Linnean Society* 112 (4): 719-734. https://doi.org/10.1111/bij.12336
Niedźwiedzki G., Brusatte S. L., Sulej T. & Butler R. J. 2014. — Basal dinosauriform and theropod dinosaurs from the mid-late Norian (Late Triassic) of Poland: implications for Triassic dinosaur evolution and distribution. *Palaeontology* 57 (6): 1121-1142. https://doi.org/10.1111/pala.12107
Owen R. 1851. — Monograph on the fossil reptilia of the Cretaceous formations. *Monographs of the Palaeontographical Society* 5 (11): 1-118. https://doi.org/10.1080/25761900.2022.12131649
Parham J. F. & Zug G. R. 1997. — Age and growth of loggerhead sea turtles (*Caretta caretta*) of Coastal Georgia: an assessment of skeletochronological age-estimates. *Bulletin of Marine Science* 61 (2): 287-304.
Peabody F. E. 1961. — Annual growth zones in living and fossil vertebrates. *Journal of Morphology* 108 (1): 11-62. https://doi.org/10.1002/jmor.1051080103
Pereyra M. E. 2023. — Comparative postcranial osteohistology and bone histovariability of aquatic and terrestrial turtles: the case of the South American *Phrynops hilarii*, *Hydromedusa tectifera* (Pleurodira, Chelidae), and *Chelonoidis chilensis* (Cryptodira, Testudinidae). *The Anatomical Record* 306 (6): 1-19. https://doi.org/10.1002/ar.25131

PETITET R., SECCHI E. R., AVENS L. & KINAS P. G. 2012. — Age and growth of loggerhead sea turtles in southern Brazil. *Marine Ecology Progress Series* 456: 255-268. https://doi.org/10.3354/meps09681

PEREYRA M. E., BONA P., CERDA I. A. & DESÁNTOLO B. 2019. — Osteohistological correlates of muscular attachment in terrestrial and freshwater Testudines. *Journal of Anatomy* 234 (6): 875-898. https://doi.org/10.1111/joa.12975

PEREYRA M. E., BONA P., CERDA I., JANNELLO J., FUENTE M. S. DE LA & DESÁNTOLO B. 2020. — Growth dynamics and body size evolution of South American long-necked chelid turtles: a bone histology approach. *Acta Palaeontologica Polonica* 65 (3): 535-545. https://doi.org/10.4202/app.00702.2019

PONTON F., ELŻANOWSKI A., CASTANET J., CHINSAMY A., DE MARGERIE E., RICQLÈS A. J. DE & CUBO J. 2004. — Variation of the outer circumferential layer in the limb bones of birds. *Acta Ornithologica* 39 (2): 137-140. https://doi.org/10.3161/068.039.0210

PRICE L. I. 1973. — Quelônio amphichelydia no Cretáceo Inferior do nordeste do Brasilá. *Revista Brasileira de Geociências* 3 (2): 84-96. https://doi.org/10.25249/0375-7536.19738496

QUEKETT J. T. 1849a. — On the intimate structure of Bone, as composing the skeleton in the four great classes of animals, viz., mammals, birds, reptiles, and fishes, with some remarks on the great value of the knowledge of such structure in determining the affinities of minute fragments of organic remains. *Transactions of the Microscopical Society of London* 2 (1): 46-58. https://doi.org/10.1111/j.1365-2818.1849.tb05102.x

QUEKETT J. T. 1849b. — Additional observations on the intimate structure of bone. *Transactions of the Microscopical Society of London* 2 (1): 40-42.

QUEKETT J. T. 1855. — *Descriptive and Illustrated Catalogue of the Histological Series Contained in the Museum of the Royal College of Surgeons of England. Prepared for the Microscope. Volume II. Structure of the Skeleton of Vertebrate Animals*. Taylor & Francis, London, 248 p.

QUENSTEDT F. A. 1889. — *Psammochelys keuperina*. (Ψάμμος Sand, χέλυς Schildkröte.). *Jahreshefte des Vereins für Vaterländische Naturkunde in Württemberg* 45: 120-130.

RHODIN A. G. J. 1985. — Comparative chondro-osseous development and growth of marine turtles. *Copeia* 1985 (3): 752. https://doi.org/10.2307/1444768

RHODIN A. G. J., OGDEN J. A. & CONLOGUE G. J. 1980. — Preliminary studies on skeletal morphology of the leatherback turtle. *Marine Turtle Newsletter* 16: 7-9.

RHODIN A. G. J., OGDEN J. A. & CONLOGUE G. J. 1981. — Chondro-osseous morphology of *Dermochelys coriacea*, a marine reptile with mammalian skeletal features. *Nature* 290 (5803): 244-246. https://doi.org/10.1038/290244a0

RHODIN J. A. G., RHODIN A. G. J. & SPOTILA J. R. 1996. — Electron microscopic of vascular cartilage canals in humeral epiphysis of hatchling leatherback, *Dermochelys coriacea*. *Chelonian Conservation and Biology* 2 (2): 250-260.

RICQLÈS A. J. DE 1976. — On bone histology of fossil and living reptiles, with comments on its functional and evolutionary significance, *in* BELLAIRS A. d'A. & COX C. B. (eds), *Morphology and Biology of Reptiles*. Linnean Society Symposium No. 3, Academic Press, New York: 123-150.

RICQLÈS A. J. DE, CASTANET J. & FRANCILLON-VIEILLOT H. 2004. — The 'message' of bone tissue in paleoherpetology. *Italian Journal of Zoology* 71 (2004): 3-12. https://doi.org/10.1080/11250000409356599

ROTHSCHILD B. M., SCHULTZE H.-P. & PELLEGRINI R. 2012. — *Herpetological osteopathology*. Springer, New York, 450 p. https://doi.org/10.1007/978-1-4614-0824-6

ROUGIER G. W., FUENTE M. S. DE LA & ARCUCCI A. B. 1995. — Late Triassic turtles from South America. *Science* 268 (5212): 855-858. https://doi.org/10.1126/science.268.5212.855

SANDER P. M. 1992. — The norian *Plateosaurus* bonebeds of central Europe and their taphonomy. *Palaeogeography, Palaeoclimatology, Palaeoecology* 93 (3-4): 255-299. https://doi.org/10.1016/0031-0182(92)90100-J

SCHEYER T. M. & CERDA I. A. 2021. — Testudines, *in* BUFFRÉNIL V. DE, RICQLÈS A. J. DE, ZYLBERBERG L. & PADIAN K. (eds), *Vertebrate Skeletal Histology and Paleohistology*. CRC Press, Boca Raton; London; New York: 385-398.

SCHEYER T. M., KLEIN N., EVERS S. W., MAUTNER A.-K. & PABST B. 2022. — First evidence of *Proganochelys quenstedtii* (Testudinata) from the Plateosaurus bonebeds (Norian, Late Triassic) of Frick, Canton Aargau, Switzerland. *Swiss Journal of Palaeontology* 141: 17.

SCHEYER T. M. & SANDER P. M. 2007. — Shell bone histology indicates terrestrial palaeoecology of basal turtles. *Proceedings of the Royal Society of London B: Biological Sciences* 247: 1885-1893. https://doi.org/10.1098/rspb.2007.0499

SCHNEIDER C. A., RASBAND W. S. & ELICERIRI K. W. 2012. — NIH Image to ImageJ: 25 years of image analysis. *Nature Methods* 9: 671-675. https://doi.org/10.1038/nmeth.2089

SCHOCH R. R. & SUES H.-D. 2015. — A Middle Triassic stem-turtle and the evolution of the turtle body plan. *Nature* 523 (7562): 584-587. https://doi.org/10.1038/nature14472

SCHOCH R. R., KLEIN N., SCHEYER T. M. & SUES H.-D. 2019. — Microanatomy of the stem-turtle Pappochelys rosinae indicates a predominantly fossorial mode of life and clarifies early steps in the evolution of the shell. *Scientific Reports* 9: 10430. https://doi.org/10.1038/s41598-019-46762-z

SCHUCHT P. J., KLEIN N. & LAMBERTZ M. 2021. — What's my age again? On the ambiguity of histology-based skeletochronology. *Proceedings of the Royal Society B: Biological Sciences* 288 (1955): 9-14. https://doi.org/10.1098/rspb.2021.1166

SCHWEIGGER A. F. 1812. — Prodromus monographiae Cheloniorum. *Königsberger Archiv für Naturwissenschaft und Mathematik* 1: 271-458.

SEELEY H. G. 1892. — On a new reptile from Welte Vreden (Beaufort West), *Eunotosaurus africanus* (Seeley). *Quarterly Journal of the Geological Society*: 583-585.

SENA M. V. A., BANTIM R. A. M., SARAIVA A. A. F., SAYÃO J. M. & OLIVEIRA G. R. 2021. — Shell and long-bone histology, skeletochronology, and lifestyle of *Araripemys barretoi* (Testudines: Pleurodira), a side-necked turtle of the lower cretaceous from Brazil. *Anais da Academia Brasileira de Ciencias* 93: 1-20. https://doi.org/10.1590/0001-3765202120201606

SNOVER M. L. 2002. — *Growth and ontogeny of sea turtles using skeletochronology: methods, validation and application to conservation*. Ph.D. thesis, Duke University, Durham, 144 p.

SNOVER M. L. & HOHN A. A. 2004. — Validation and interpretation of annual skeletal marks in loggerhead (*Caretta caretta*) and Kemp's ridley (*Lepidochelys kempii*) sea turtles. *Fishery Bulletin* 102 (4): 682-692.

SNOVER M. L. & RHODIN A. G. J. 2008. — Comparative ontogenetic and phylogenetic aspects of chelonian chondro-osseous growth and skeletochronology, *in* WYNEKEN J., GODFREY M. H. & BELS V. (eds), *Biology of Turtles*. CRC Press, Boca Raton; London; New York: 17-43.

SNOVER M. L., AVENS L. & HOHN A. A. 2007a. — Back-calculating length from skeletal growth marks in loggerhead sea turtles *Caretta caretta*. *Endangered Species Research* 3: 95-104. https://doi.org/10.3354/esr003095

SNOVER M. L., HOHN A. A., CROWDER L. B. & HEPPELL S. S. 2007b. — Age and growth in Kemp's ridley sea turtles: evidence from mark-recapture and skeletochronology, *in* PLOTKIN P. T. (ed.), *Biology and Conservation of Ridley sea turtles*. John Hopkins University Pres, Baltimore: 89-104.

STAESCHE K. 1929. — Schildkröteneste aus der oberen Kreide Patagoniens. *Palaeontographica* 72: 103-123.

STERLI J., FUENTE M. S. DE LA & ROUGIER G. W. 2007. — Anatomy and relationships of *Palaeochersis talampayensis*, a Late Triassic turtle from Argentina. *Palaeontographica Abteilung A* 281 (1-3): 1-61. https://doi.org/10.1127/pala/281/2007/1

Sterli J., Martínez R. N., Cerda I. A. & Apaldetti C. 2021. — Appearances can be deceptive: bizarre shell microanatomy and histology in a new Triassic turtle (Testudinata) from Argentina at the dawn of turtles. *Papers in Palaeontology* 7 (2): 1097-1132. https://doi.org/10.1002/spp2.1334

Sulej T., Niedźwiedzki G. & Bronowicz R. 2012. — A new Late Triassic vertebrate fauna from Poland with turtles, aetosaurs, and coelophysoid dinosaurs. *Journal of Vertebrate Paleontology* 32 (5): 1033-1041. https://doi.org/10.1080/02724634.2012.694384

Suzuki H. K. 1963. — Studies on the osseous system of the slider turtle. *Annals of the New York Academy of Sciences* 109 (1): 351-410. https://doi.org/10.1111/j.1749-6632.1963.tb13476.x

Szczygielski T. 2017. — Homeotic shift at the dawn of the turtle evolution. *Royal Society Open Science* 4: 160933. https://doi.org/http://dx.doi.org/10.1098/rsos.160933

Szczygielski T. & Sulej T. 2016. — Revision of the Triassic European turtles *Proterochersis* and *Murrhardtia* (Reptilia, Testudinata, Proterochersidae), with the description of new taxa from Poland and Germany. *Zoological Journal of the Linnean Society* 177 (2): 395-427. https://doi.org/10.1111/zoj.12374

Szczygielski T. & Sulej T. 2019. — The early composition and evolution of the turtle shell (Reptilia, Testudinata). *Palaeontology* 62 (3): 375-415. https://doi.org/10.1111/pala.12403

Szczygielski T. & Słowiak J. 2022. — Shell histology of the Triassic turtle, *Proterochersis porebensis*, provides novel insights about shell ankylosis. *Comptes Rendus Palevol* 21 (29): 619-679. https://doi.org/10.5852/cr-palevol2022v21a29

Szczygielski T., Słowiak J. & Dróżdż D. 2018. — Shell variability in the stem turtles *Proterochersis* spp. *PeerJ* 6: e6134. https://doi.org/10.7717/peerj.6134

Szulc J. & Racki G. 2015. — Grabowa Formation – the basic lithostratigraphic unit of the Upper Silesian Keuper. *Przeglad Geologiczny* 63 (2): 103-113.

Szulc J., Racki G., Jewuła K. & Środoń J. 2015. — How many Upper Triassic bone-bearing levels are there in Upper Silesia (Southern Poland)? A critical overview of stratigraphy and facies. *Annales Societatis Geologorum Poloniae* 85 (4): 587-626. https://doi.org/10.14241/asgp.2015.037

Turner Tomaszewicz C. N., Seminoff J. A., Avens L., Goshe L. R., Peckham S. H., Rguez-Baron J. M., Bickerman K. & Kurle C. M. 2015. — Age and residency duration of loggerhead turtles at a North Pacific bycatch hotspot using skeletochronology. *Biological Conservation* 186: 134-142. https://doi.org/10.1016/j.biocon.2015.03.015

Valastro C., Di Comite M., Paci S., Franchini D., Ciccarelli S. & Di Bello A. 2023. — Bone healing process of a multiple humeral fracture in a *Caretta caretta*: clinical, surgical, radiographic and histomorphometric assessments. *Animals* 13 (3): 376. https://doi.org/10.3390/ani13030376

Vandelli D. 1761. — *Epistola de holothurio, et testudine coriacea ad celebrrimum Carolum Linnaeum*. Padova, Conzatti. 12 p.

Wallis K. 1927. — Zur Knochenhistologie und Kallusbildung beim Reptil (*Clemys leprosa* Schweigg.). *Zeitschrift für Zellforschung und Mikroskopische Anatomie* 6 (1): 1-26. https://doi.org/10.1007/BF02583432

Werneburg I., Kyriakouli C. & Szczygielski T. 2022. — A surface scan of the 'Tübingen Steinkern', Holotype of *Proganochelys quenstedtii* (Testudinata), with some historical remarks. *MorphoMuseuM* 8 (3): e168. https://doi.org/10.18563/journal.m3.168

Wieland G. R. 1896. — *Archelon ischyros*: a new gigantic cryptodire testudinate from the Fort Pierre Cretaceous of South Dakota. *American Journal of Science* 2 (12): 399-412.

Williston S. W. 1894. — A new turtle from the Benton Cretaceous. *The Kansas University Quarterly* 3: 5-18.

Wilson L. E. 2023. — Rapid growth in Late Cretaceous sea turtles reveals life history strategies similar to extant leatherbacks. *PeerJ* 11: e14864. https://doi.org/10.7717/peerj.14864

Wood R. C. 1976. — *Stupendemys geographicus*, the world's largest turtle. *Breviora* 436: 1-31.

Zahner M. & Brinkmann W. 2019. — A Triassic averostran-line theropod from Switzerland and the early evolution of dinosaurs. *Nature Ecology and Evolution* 3 (8): 1146-1152. https://doi.org/10.1038/s41559-019-0941-z

Zug G. R. 1990. — Age determination of long-lived reptiles: some techniques for seaturtles. *Annales des Sciences Naturelles, Zoologie* 11: 219-222.

Zug G. R. & Balazs G. H. 1985. — Skeletochronological age estimates for Hawaiian green turtles. *Marine Turtle Newsletter* 33: 9-10.

Zug G. R. & Parham J. F. 1996. — Age and growth in leatherback turtles, *Dermochelys coriacea* (Testudines: Dermochelyidae): a skeletochronological analysis. *Chelonian Conservation and Biology* 2 (2): 244-249.

Zug G. R. & Glor R. E. 1998. — Estimates of age and growth in a population of green sea turtles (*Chelonia mydas*) from the Indian River lagoon system, Florida: a skeletochronological analysis. *Canadian Journal of Zoology* 76 (8): 1497-1506. https://doi.org/10.1139/z98-090

Zug G. R., Wynn A. H. & Ruckdeschel C. 1986. — Age determination of loggerhead sea turtles, *Caretta caretta*, by incremental growth marks in the skeleton. *Smithsonian Contributions to Zoology* (427): 1-34.

Zug G. R., Balazs G. H. & Wetherall J. A. 1995. — Growth in juvenile loggerhead seaturtles (*Caretta caretta*) in the north Pacific pelagic habitat. *Copeia* 1995 (2): 484-487. https://doi.org/10.2307/1446917

Zug G. R., Kalb H. J. & Luzar S. J. 1997. — Age and growth in wild Kemp's ridley seaturtles *Lepidochelys kempii* from skeletochronological data. *Biological Conservation* 80 (3): 261-268. https://doi.org/10.1016/S0006-3207(96)00143-7

Zug G. R., Balazs G. H., Wetherall J. A., Parker D. M. & Murakawa S. K. K. 2002. — Age and growth of Hawaiian green seaturtles (*Chelonia mydas*): an analysis based on skeletochronology. *Fishery Bulletin* 100 (1): 117-127.

Zug G. R., Chaloupka M. & Balazs G. H. 2006. — Age and growth in olive ridley seaturtles (*Lepidochelys olivacea*) from the North-central Pacific: a skeletochronological analysis. *Marine Ecology* 27 (3): 263-270. https://doi.org/10.1111/j.1439-0485.2006.00109.x

Submitted on 22 February 2023;
accepted on 9 June 2023;
published on 6 November 2023.

APPENDIX 1. — Measurements and length estimations of femora of *Proterochersis porebensis* Szczygielski & Sulej, 2016. Abbreviations: **DD**, distal depth; **DW**, distal width; **L**, length; **LP**, length as preserved; **PW**, proximal width; **PWP**, proximal width as preserved; **PD**, proximal depth.

ZPAL V. 39/	L (mm)	LP (mm)	DW (mm)	DD (mm)	PW (mm)	PWP (mm)	PD (mm)	DW/DD	L/DW	L/DD	L/PW	PW/PD	L/PD	Estimated length				Used for
														DW (mm)	DD (mm)	PW (mm)	PD (mm)	
26	–	50	40	18	–	–	–	2.222222	–	–	–	–	–	116.33019	100.41608	0	0	–
48	127	–	40	22	39	–	36	1.818182	3.175	5.772727	3.25641	1.083333333	3.527778	116.33019	122.73077	121.58511	118.28261	–
52	–	35	–	–	19	–	21	–	–	–	–	0.904761905	–	0	0	59.23377	68.998188	–
166	–	23	–	–	–	35	33	–	–	–	–	1.060606061	–	0	0	109.11484	108.42572	–
216	–	26	26	12	–	–	–	2.166667	–	–	–	–	–	75.614623	66.944056	0	0	–
217	–	27	18	9	–	–	–	2	–	–	–	–	–	52.348585	50.208042	0	0	–
432	140	–	53	26	47	–	46	2.038462	2.6415094	5.384615	2.978723	1.02173913	3.043478	154.1375	145.04545	146.52564	151.13889	CT
434	–	38	25	11	–	–	–	2.272727	–	–	–	–	–	72.706368	61.365385	0	0	–
435	–	24	–	–	–	18	20	–	–	–	–	0.9	–	0	0	56.116203	65.71256	–
499	–	27	21	10	–	–	–	2.1	–	–	–	–	–	61.073349	55.786713	0	0	Histology
500	–	66	49	23	–	–	–	2.130435	–	–	–	–	–	142.50448	128.30944	0	0	Histology
Standard deviation								0.14294	0.3772348	0.274437	0.196354	0.086581854	0.342451	–	–	–	–	–
Mean								2.093587	2.9082547	5.578671	3.117567	0.994088086	3.285628	–	–	–	–	–

Appendix 2. — Distal width (**DW**) to distal depth (**DD**) ratios for *Proterochersis porebensis* Szczygielski & Sulej, 2016 femora (all ZPAL V. 39/).

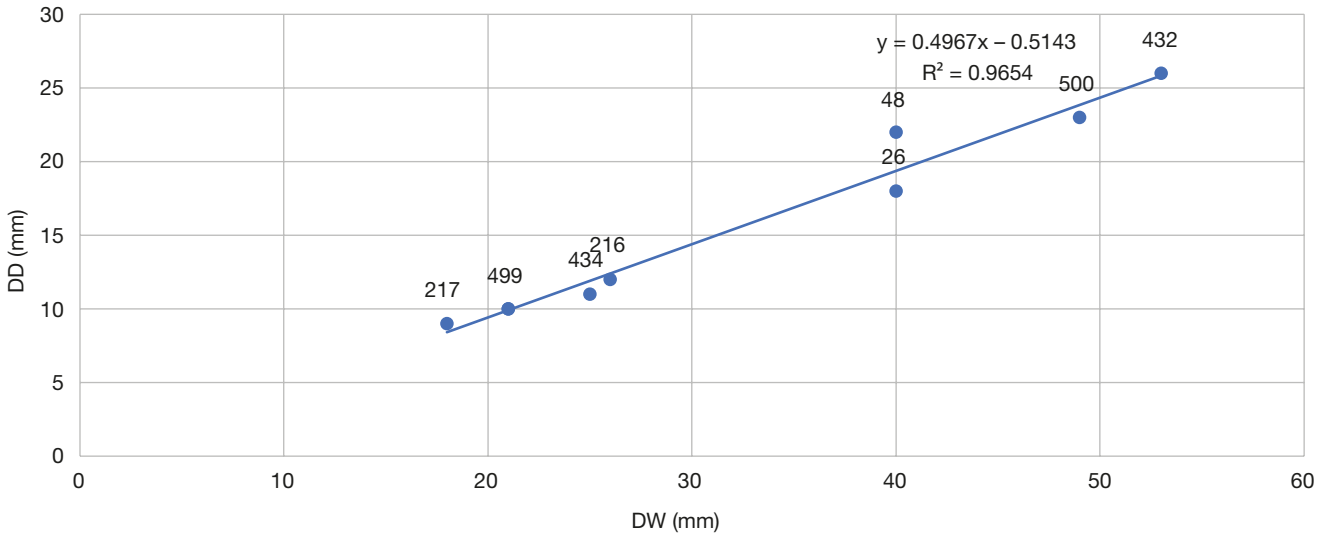

APPENDIX 3. — Lenghts of femora of *Proterochersis porebensis* Szczygielski & Sulej, 2016 estimated based on mean distal depth to bone length ratio and based on extrapolation from complete specimens.

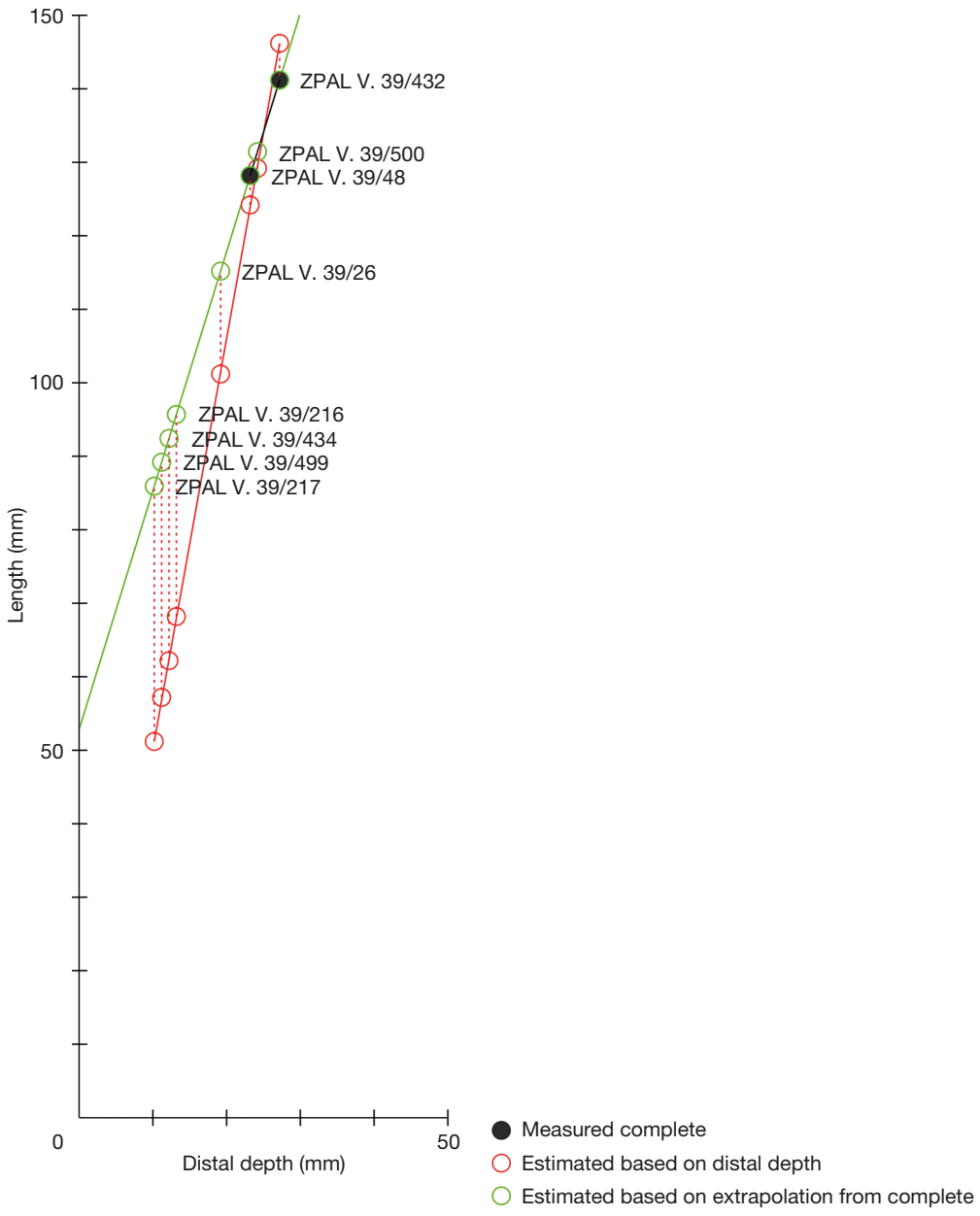

APPENDIX 4. — Measurements and length estimations of humeri of *Proterochersis porebensis* Szczygielski & Sulej, 2016. Abbreviations: Distal depth (DD); Distal width (DW; **L**, length; **LP**, length as preserved; **PW**, proximal width; **PWP**, proximal width as preserved.

											Estimated length		
ZPAL V.39/	**L (mm)**	**LP (mm)**	**DW (mm)**	**DD (mm)**	**PW (mm)**	**PWP (mm)**	**DW/DD**	**L/DW**	**L/DD**	**L/PW**	**DW (mm)**	**DD (mm)**	**Used for**
50	106	–	46	18	–	50	2.555555556	2.3043478	5.888889		113.3555556	105.6717949	CT
156	77	–	30	13	39	–	2.307692308	2.5666667	5.923077	1.974359	73.92753623	76.31851852	CT
433	–	38	34	14	–	–	2.428571429	–	–	–	83.78454106	82.18917379	Histology
439	–	22	20	8	–	–	2.5	–	–	–	49.28502415	46.96524217	Histology
446	58	–	23	10	27	–	2.3	2.5217391	5.8	2.148148	56.67777778	58.70655271	CT
Standard deviation							0.113851231	0.1402906	0.063532	0.122888	–	–	–
Mean							2.418363858	2.4642512	5.870655	2.061254	–	–	–

Appendix 5. — Distal width (**DW**). distal depth (**DD**) and proximal width (**PW**) ratios to bone length (**L**) for humeri of *Proterochersis porebensis* Szczygielski & Sulej, 2016 (all ZPAL V. 39/).

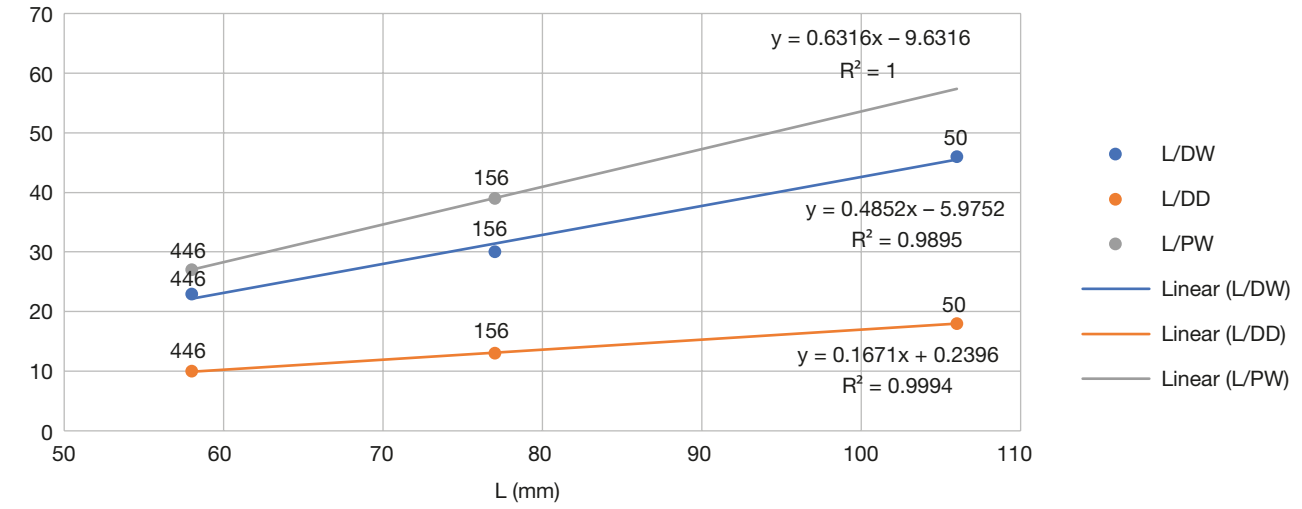

Appendix 6. — Distal width (**DW**) to distal depth (**DD**) ratios for *Proterochersis porebensis* Szczygielski & Sulej, 2016 humeri (all ZPAL V. 39/).

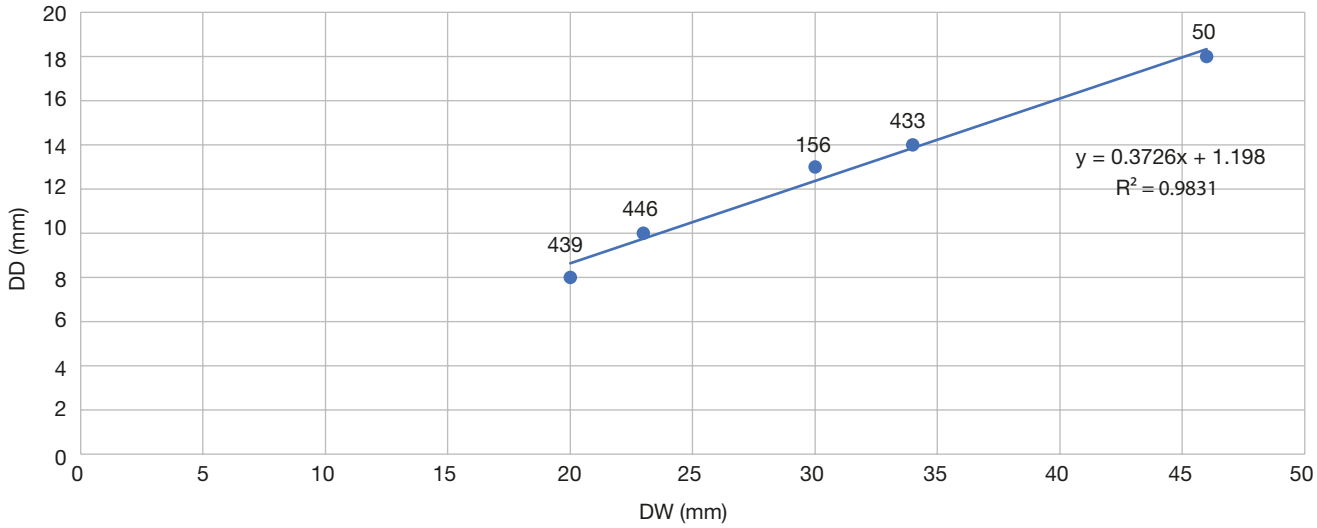

Appendix 7. — Measurements of stylopodial bones and estimations of carapace lengths of *Proterochersis porebensis* Szczygielski & Sulej, 2016.

Species	Specimen	Log midline carapace length	Side	Log humerus length	Log femur length
Palaeochersis talampayensis Rougier, Fuente & Arcucci, 1995	PULR 068	1.658011397	Left	1.10	–
			Right	1.079181246	–
Proganochelys quenstedtii Baur, 1887	SMNS 16980	1.685741739	Left	1.127104798	1.184691431
			Right	1.1430148	–
	SMNS 17203	1.602059991	Left	–	1.117271296
	SMNS 17204	1.698970004	Left	–	1.198657087
			Right	–	1.201397124
	SMF 09-F2	1.740362689	Left	1.193124598	–
Proterochersis porebensis Szczygielski & Sulej, 2016	ZPAL V. 39/48	1.596597096	Right	–	1.103803721

APPENDIX 8. — Log of humerus length (**L**) to log of midline carapace length (**MiCL**) for *Palaeochersis talampayensis* Rougier, Fuente & Arcucci, 1995 and *Proganochelys quenstedtii* Baur, 1887.

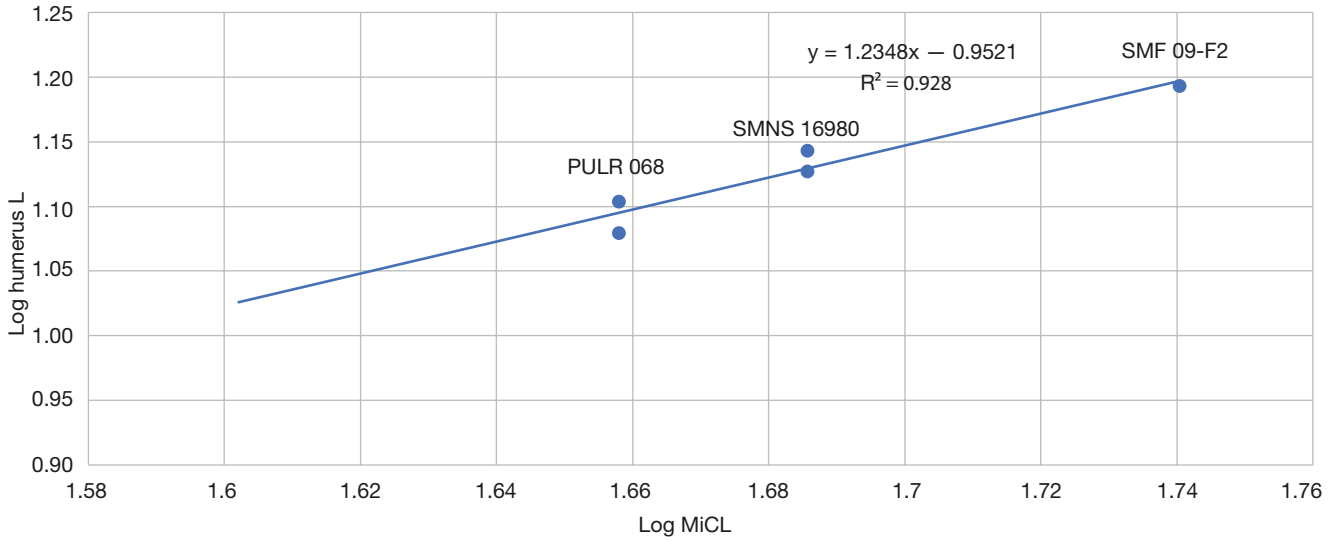

APPENDIX 9. — Bivariate linear fit (PAST) of the log of humerus length (**L**) to log of midline carapace length (**MiCL**) for *Palaeochersis talampayensis* Rougier, Fuente & Arcucci, 1995 and *Proganochelys quenstedtii* Baur, 1887.

Ordinary Least Squares Regression			
Slope a	1.258	**Standard error a**	0.18778
t	6.6995	**p (slope)**	0.0067851
Intercept b	–0.99199	**Standard error b**	0.31656
95% bootstraped confidence intervals (N = 1999)			
Slope a	(0.35752, 1.5386)		
Intercept b	(–1.4634, 0.51567)		
Correlation			
r	0.96817		
r²	0.93735		
t	6.6995		
p (uncorrected)	0.0067851	**Permutation p**	0.0343

APPENDIX 10. — Log humerus length (**L**) to log midline carapace length (**MiCL**) for *Proganochelys quenstedtii* Baur, 1887 only.

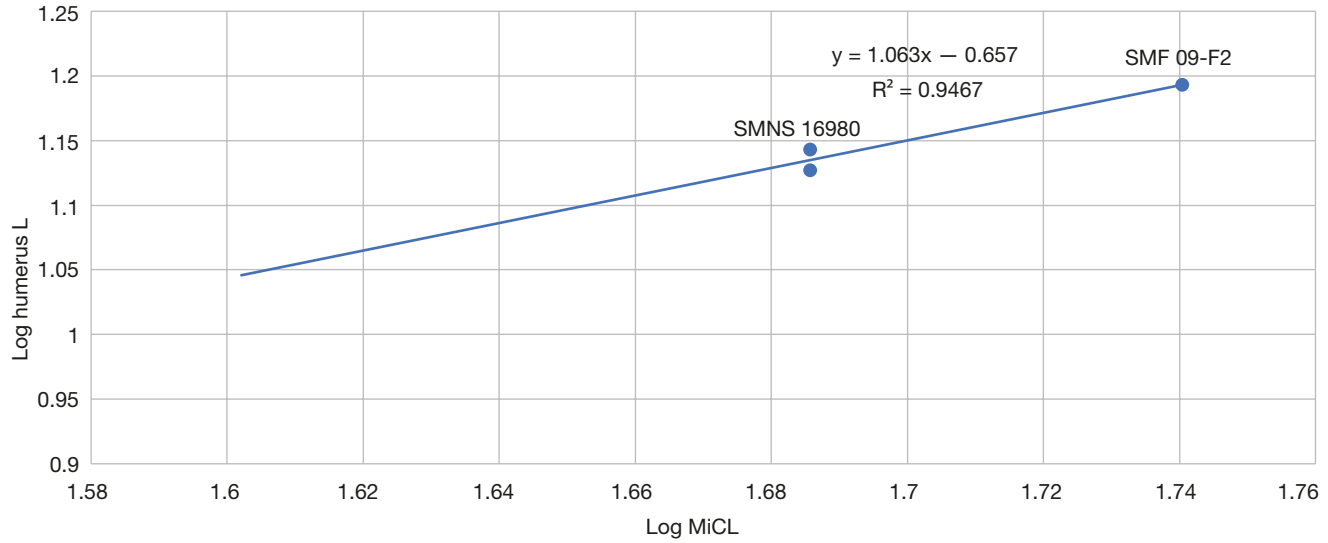

Appendix 11. — Bivariate linear fit (PAST) of the log of humerus length (**L**) to log of midline carapace length (**MiCL**) for *Proganochelys quenstedtii* Baur, 1887.

Ordinary Least Squares Regression			
Slope a	1.063	**Standard error a**	0.25226
t	4.2142	**p (slope)**	0.14832
Intercept b	–0.65697	**Standard error b**	0.42988
95% bootstraped confidence intervals (N = 1999)			
Slope a	(0.91741, 5.3734E15)		
Intercept b	(–9.3516E15, 0.4035)		
Correlation			
r	0.97298		
r²	0.94669		
t	4.2142		
p (uncorrected)	0.14832	**Permutation p**	0.3389

Appendix 12. — Log femur length (**L**) to log midline carapace length (**MiCL**) for *Palaeochersis talampayensis* Rougier, Fuente & Arcucci, 1995, *Proganochelys quenstedtii* Baur, 1887, and *Proterochersis porebensis* Szczygielski & Sulej, 2016 (values for missing bones duplicated from contralateral side of the body).

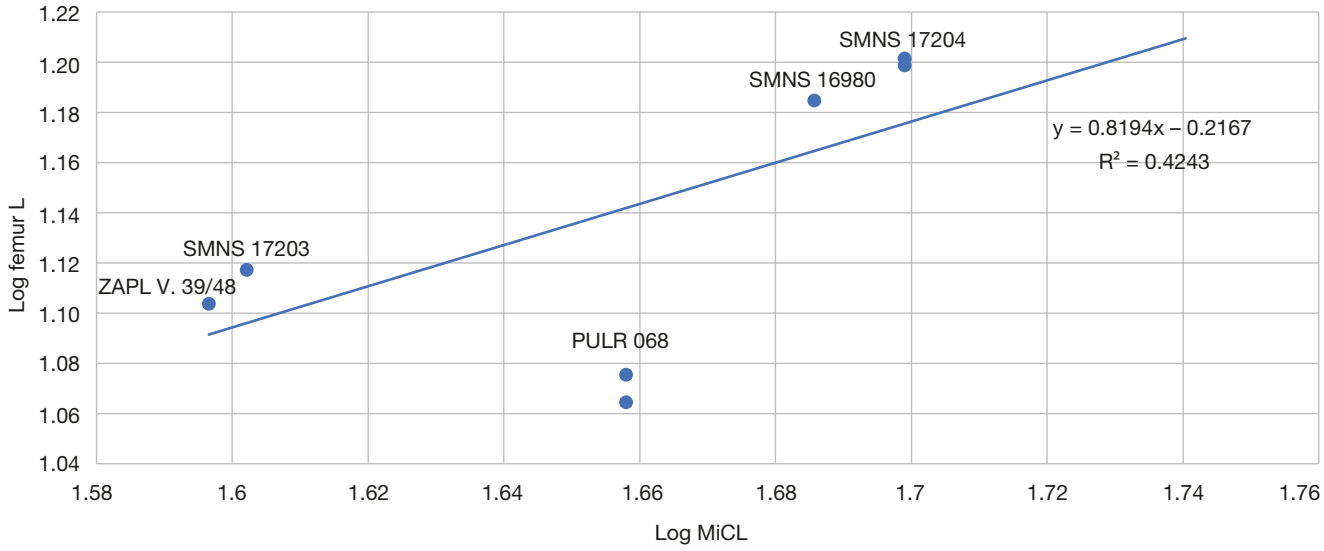

Appendix 13. — Log femur length (**L**) to log midline carapace length (**MiCL**) for *Proganochelys quenstedtii* Baur, 1887 and *Proterochersis porebensis* Szczygielski & Sulej, 2016 (values for missing bones duplicated from contralateral side of the body).

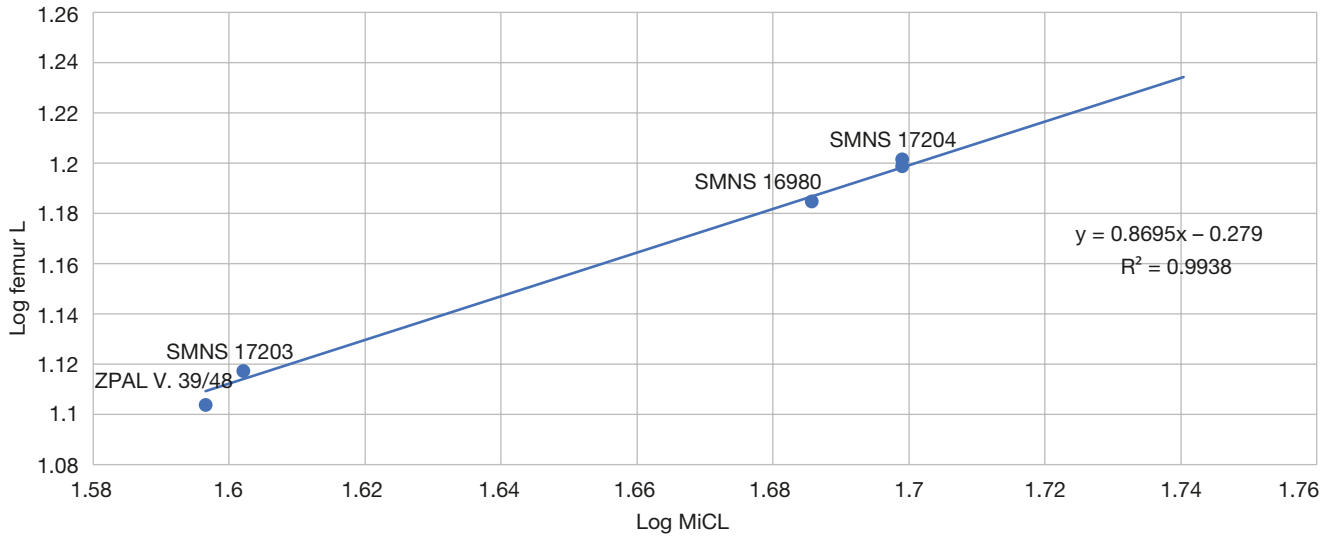

Appendix 14. — Bivariate linear fit (PAST) log femur length (**L**) to log midline carapace length (**MiCL**) for *Proganochelys quenstedtii* Baur, 1887 and *Proterochersis porebensis* Szczygielski & Sulej, 2016.

Ordinary Least Squares Regression			
Slope a	0.89106	**Standard error a**	0.038666
t	23.045	**p (slope)**	0.00017899
Intercept b	–0.31484	**Standard error b**	0.064075
95% bootstraped confidence intervals (N = 1999)			
Slope a	(0.58828, 0.96098)		
Intercept b	(–0.4313, 0.19812)		
Correlation			
r	0.99719		
r²	0.99438		
t	23.045		
p (uncorrected)	0.00017899	**Permutation p**	0.0167

Appendix 15. — Log femur length (**L**) to log midline carapace length (**MiCL**) for Proganochelys quenstedtii only (values for missing bones duplicated from contralateral side of the body).

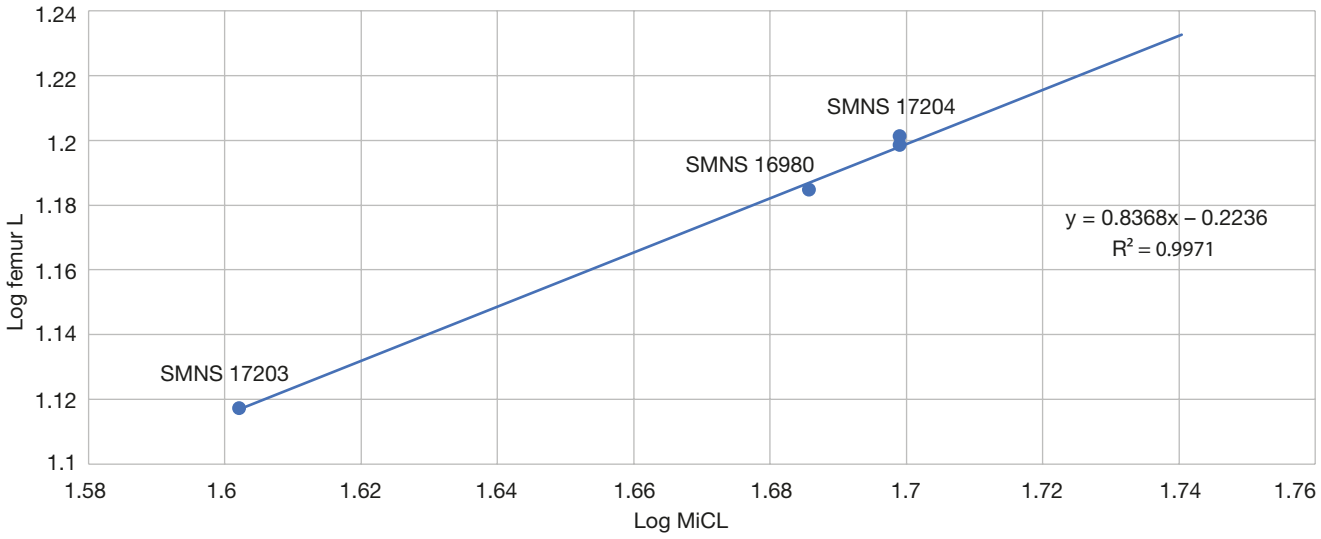

Appendix 16. — Bivariate linear fit (PAST) log femur length (**L**) to log midline carapace length (**MiCL**) for *Proganochelys quenstedtii* Baur, 1887.

Ordinary Least Squares Regression			
Slope a	0.8451	**Standard error a**	0.034419
t	24.554	**p (slope)**	0.0016546
Intercept b	–0.23703	**Standard error b**	0.057454
95% bootstraped confidence intervals (N = 1999)			
Slope a	(0.42732, 0.88453)		
Intercept b	(–0.30059, 0.147014)		
Correlation			
r	0.99835		
r²	0.99669		
t	24.554		
p (uncorrected)	0.0016546	**Permutation p**	0.0821